HHS Public Access

Author manuscript

Science. Author manuscript; available in PMC 2015 December 19.

Published in final edited form as:

Science. 2015 June 19; 348(6241): aaa8205. doi:10.1126/science.aaa8205.

A mucosal vaccine against *Chlamydia trachomatis* generates two waves of protective memory T cells

Georg Stary[#1,*], **Andrew Olive**[#1], **Aleksandar F. Radovic-Moreno**[#2,3], **David Gondek**[1], **David Alvarez**[1], **Pamela A. Basto**[2,3], **Mario Perro**[1], **Vladimir D. Vrbanac**[4], **Andrew M. Tager**[4], **Jinjun Shi**[6], **Jeremy A. Yethon**[5], **Omid C. Farokhzad**[6,7], **Robert Langer**[2,3], **Michael N. Starnbach**[1], and **Ulrich H. von Andrian**[1,8,*]

[1] Division of Immunology, Department of Microbiology and Immunobiology, Harvard Medical School, Boston, MA 02115, USA.

[2] Harvard-MIT Division of Health Sciences & Technology, Cambridge, MA 02139, USA.

[3] Department of Chemical Engineering, Massachusetts Institute of Technology, Cambridge, MA 02139, USA.

[4] The Center for Immunology and Inflammatory Diseases, Massachusetts General Hospital, Harvard Medical School, Boston, MA 02114, USA.

[5] Sanofi Pasteur, Cambridge MA 02139, USA.

[6] Laboratory of Nanomedicine and Biomaterials, Department of Anesthesiology, Brigham and Women's Hospital, Harvard Medical School, Boston, MA 02115, USA.

[7] King Abdulaziz University, Jeddah, Saudi Arabia.

[8] The Ragon Institute of MGH, MIT and Harvard, Cambridge, MA 02139, USA.

[#] These authors contributed equally to this work.

Abstract

Genital *Chlamydia trachomatis* (*Ct*) infection induces protective immunity that depends on interferon-γ producing CD4 T-cells. By contrast, mucosal exposure to ultraviolet light (UV)-inactivated *Ct* (UV-*Ct*) generated regulatory T-cells that exacerbated subsequent *Ct* infection. We show that mucosal immunization with UV-*Ct* complexed with charge-switching synthetic adjuvant particles (cSAP) elicited long-lived protection in conventional and humanized mice. UV-*Ct*-cSAP targeted immunogenic uterine $CD11b^{+}CD103^{-}$ dendritic cells (DCs), whereas UV-*Ct* accumulated in tolerogenic $CD11b^{-}CD103^{+}$ DCs. Regardless of vaccination route, UV-*Ct*-cSAP induced systemic memory T-cells, but only mucosal vaccination induced effector T-cells that rapidly seeded uterine mucosa with resident memory T-cells (T_{RM}). Optimal *Ct* clearance required both T_{RM} seeding and subsequent infection-induced recruitment of circulating memory T-cells.

[*] Correspondence to: Ulrich H. von Andrian, M.D.: uva@hms.harvard.edu or Georg Stary, M.D.: georg_stary@hms.harvard.edu.

One Sentence Summary:

Mucosal vaccination with inactivated *C. trachomatis* linked to adjuvant nanocarriers elicits two memory T cell subsets that protect against uterine *C. trachomatis* infection.

Thus, UV-*Ct*-cSAP vaccination generated two synergistic memory T-cell subsets with distinct migratory properties.

Graphical Abstract

Protection against *C. trachomatis* infection after mucosal UV-*Ct*–cSAP vaccination. Upon mucosal vaccination, dendritic cells carry UV-*Ct*–cSAP to lymph nodes and stimulate CD4 T cells. Effector T cells are imprinted to traffic to uterine mucosa (1st wave) and establish tissue-resident memory cells (T_{RM}). Vaccination also generates circulating memory T cells. Upon genital *Ct* infection, local reactivation of uterine T_{RM} triggers the recruitment of the circulating memory subset (2nd wave). Optimal pathogen clearance requires both waves of memory cells.

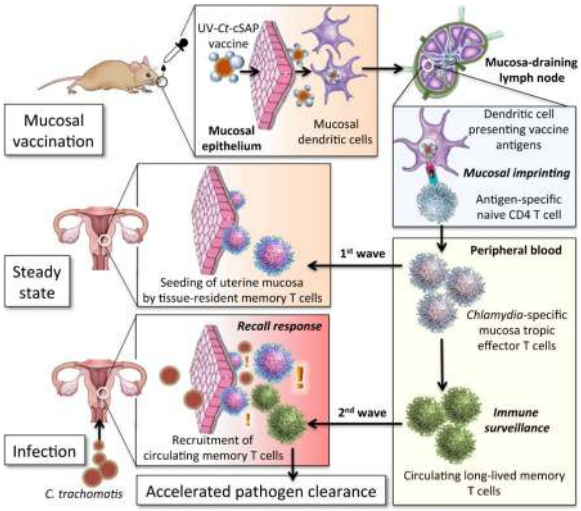

INTRODUCTION

Although subcutaneous (s.c.) or intramuscluar (i.m.) vaccination can generate efficient systemic and cutaneous immunity against many pathogens, vaccination by these non-mucosal routes often induces little or no protection at mucosal surfaces (1). A reason for this shortcoming is thought to be the differential imprinting of activated effector/memory lymphocytes in regional lymphoid tissues. These organs are populated by specialized antigen (Ag) presenting dendritic cells (DCs) that induce the expression of tissue-specific homing receptors in T and B cells (2-4). Acquisition of tissue tropism enables the preferential migration of Ag-experienced lymphocytes to regions of the body that are associated with the secondary lymphoid organs where Ag was first encountered (2, 3, 5-11). Thus, while intra- or subcutaneous and i.m. vaccines act in peripheral lymph nodes (LNs) to induce primarily skin-homing memory cells, mucosal vaccine exposure targets Ags into mucosa-associated lymphoid tissues (MALT) and focuses the ensuing memory response toward mucosal surfaces (6, 12-16). However, only a handful of mucosal vaccines are currently available for use in humans, and most of these vaccines consist of replicating microorganisms, which may themselves cause infections in vulnerable individuals (17). Such safety concerns could be avoided with non-replicating vaccines, such as killed pathogens or inanimate Ags, however, mucosal exposure to non-infectious Ags is typically

insufficient to elicit a protective immune response unless the Ags are combined with potent adjuvants that are often too toxic for use in humans (18, 19).

These immunobiological challenges present formidable obstacles to the development of effective vaccines for many mucosal pathogens. One prominent example among these 'intractable' pathogens is *Chlamydia trachomatis* (*Ct*), a gram-negative obligatory intracellular bacterium that infects mucosal epithelial cells. *Ct* is the most common sexually transmitted bacterial pathogen and the leading cause of female infertility, ectopic pregnancy (20-22) and infectious blindness worldwide (23). Clinical trials in the 1960's with inactivated elementary bodies (EBs), the infectious form of *Ct* (24), achieved partial early protection, but at later stages some vaccinated individuals experienced more severe symptoms upon ocular *Ct* exposure than placebo recipients (24-30). The underlying mechanism for this apparently enhanced risk of *Ct*-induced pathology following exposure to killed *Ct* is not understood. To this day, this persistent uncertainty has stymied further clinical development of *Ct* vaccines.

RESULTS & DISCUSSION

Effect of uterine mucosal exposure to live and killed *Ct*

Here, we have used mice to explore the immunological consequences of mucosal exposure to live or killed *Ct* by performing intra-uterine (i.u.) inoculations of either infectious *Ct* (serovar L2 unless stated otherwise) or ultraviolet light-inactivated *Ct* (UV-*Ct*). The animals were re-challenged with live *Ct* four weeks later and uterine bacterial burden was assessed after 6 days (**Fig. 1A**). Consistent with earlier observations in this model (31), mice that had been previously infected with *Ct* acquired protective immunity as evidenced by a ~50-fold reduction in bacterial burden upon reinfection as compared to naive controls (**Fig. 1B**). In contrast, the bacterial burden in infected mice that had been previously exposed to UV-*Ct* was 5- to 10-fold greater than in the non-immunized group. This exacerbated susceptibility to infection in the UV-*Ct* group was intriguingly reminiscent of the reported outcome of human vaccine trials five decades ago (25-29) and suggested that inactivated *Ct* was not merely ‘invisible’ to the host immune system, but somehow promoted tolerance.

Having thus determined that mucosal exposure to UV-*Ct* induces a pronounced tolerogenic immune response in mice, we asked whether mixing UV-*Ct* with an adjuvant could convert UV-*Ct* into an immunogen that might elicit protective immunity. However, i.u. injection of UV-*Ct* mixed with alum or with two different TLR agonists, imiquimod (TLR7 ligand) or CpG (TLR9 ligand), not only failed to confer protection, but also rendered mice more susceptible to reinfection, similar to UV-*Ct* alone (**Fig. 1C**). Interestingly, when mice were instead immunized by s.c. injection, UV-*Ct* provoked neither a tolerogenic response nor did it confer measurable protection, even when combined with adjuvants. Thus, the route of immunization can determine not only the tissue-tropism of effector/memory cells, but apparently also the tolerogenicity of a given Ag.

Conjugation of UV-inactivated *Ct* to charge-switching synthetic adjuvant particles

In light of these observations, we speculated that the lack of immunogenicity of i.u. exposure to crude mixtures of adjuvants with UV-*Ct* may have been due to differential permeability of the intact mucosal barrier to UV-*Ct* and/or free adjuvants. Thus, we reasoned that physical linkage of an adjuvant to UV-*Ct* may be necessary to allow both vaccine components to cross the epithelial barrier and be acquired by the same submucosal immunogenic DCs. To test this idea, we engineered modified charge-switching synthetic particles (cSPs), biodegradable nanocarriers that were developed recently to target encapsulated antibiotics to bacterial surfaces (32). Using an emulsion-based manufacturing process, cSPs self-assemble from a tri-block co-polymer, poly(*D,L*-lactic-co-glycolic acid)-b-poly(*L*-histidine)-bpoly(ethylene glycol) (PLGA-PLH-PEG) to form a hydrophobic core (PLGA) and a bilayered hydrophilic surface consisting of an inner layer of PLH and an outer layer of PEG (32). At physiologic pH7.4 cSPs carry a slight negative surface charge, but acidification to below pH6.5 induces protonation of PLH imidazole groups, rendering cSPs cationic and allowing them to form conjugates with negatively charged bacteria (32). For use in vaccines, we modified cSPs by incorporating a second hydrophobic polymer, poly(*D,L*-lactic acid), that was covalently coupled to R848 (a.k.a. resiquimod), a potent TLR7/8 agonist (PLA-R848). Recent work has shown that following s.c. injection into mice PEGylated PLA-R848 containing nanoparticles are phagocytosed by DCs and release free R848 within endosomes resulting in efficient activation of endosomal TLR7 and DC maturation, while minimizing systemic exposure to this adjuvant (33). Thus, by incorporating R848 into cSPs, we created charge-switching synthetic adjuvant particles (cSAPs) that were then mixed with UV-*Ct* EBs in aqueous buffer (**Fig. 1D**). Following acidification, cSAPs formed conjugates with UV-*Ct*, as confirmed by flow cytometry (**Figs. 1E, F**), transmission electron microscopy (**Fig. 1G**) and dynamic light scattering analysis (**Fig. 1H**). By contrast, synthetic adjuvant particles (SAPs) that lacked PLH and could not undergo surface-charge switching failed to bind *UV-Ct* and were used as a control.

Effect of uterine mucosal vaccination with UV-*Ct*-cSAP conjugates

Having verified that cSAPs serve as an effective tool to attach a potent small molecule adjuvant, R848, to UV-*Ct* we compared the effect of i.u. exposure to UV-*Ct* alone or UV-*Ct* mixed with free SAPs (UV-*Ct* + SAP) or conjugated with either cSAPs (UV-*Ct*–cSAP) or adjuvant-free cSPs (UV-*Ct*– cSP) using the same i.u. prime/challenge protocol as above. Again, pre-conditioning with UV-*Ct* rendered mice hypersusceptible to subsequent *Ct* challenge, and this tolerogenic effect was preserved in animals that had received UV-*Ct* + SAP or UV-*Ct*–cSPs (**Fig. 2A**). By contrast, bacterial clearance was dramatically accelerated in mice that had been immunized with UV-*Ct*–cSAP (**Fig. 2B**). Remarkably, the extent of vaccine-induced protection was equivalent, if not superior, when compared to animals with ‘natural’ memory after previous *Ct* infection. These results were independently confirmed when uteri of challenged mice were analyzed by blinded observers for the presence of infectious *Ct* by *in vitro* testing of tissue extracts for inclusion-forming units in McCoy cells (**Figs. 2C, S1**). Robust protection was also achieved when cSAPs were conjugated to formalin-inactivated *Ct* (not shown) or to another UV-inactivated strain of *Ct*, serotype E (*Ct-E*) (**Fig. S2**), or to *C. muridarum* (*Cm*), a mouse adapted strain (**Fig. 2D**).

Of note, while pathological changes in murine uteri infected with human adapted strains of *Ct* are variable, infection of naive mice with *Cm* caused reproducible tissue damage resulting in accumulation of serous exudate in fallopian tubes (hydrosalpinx), reminiscent of the pathology induced by chronic *Ct* infection in humans. By contrast, animals that had received i.u. UV-*Cm*-cSAP vaccination were profoundly protected against hydrosalpinx formation when compared to naive animals or recipients of UV-*Cm* alone (**Fig. 2E**).

Importantly, the differential effects of i.u. conditioning with UV-*Ct*–cSAP and UV-*Ct* persisted unabated for at least 6 months; the former continued to afford profound protection, while the latter predisposed to enhanced susceptibility to *Ct* rechallenge, indicating that mucosal exposure to UV-*Ct* in both immunogenic and tolerogenic contexts elicits sustained and qualitatively unchanging memory (**Fig. 2F**).

UV-*Ct*-cSAP vaccination induces *Ct* specific protective T-helper 1 memory cells

In light of the fact that the charge-based conjugation of cSAPs to UV-*Ct* was apparently sufficient not only to permanently avert the default tolerance response to UV-*Ct*, but also to produce robust long-term protective immunity that prevented infection-induced tissue damage, we set out to dissect the underlying immunological mechanisms. Recent clinical evidence suggests that humans develop at least partially protective immunity upon clearance of genital *Ct* infection, whereby interferon (IFN)-γ production, presumably by T-helper 1 (T_{H1}) cells, was inversely correlated with the risk for reinfection (34-36). Although mechanistic information in humans is sparse and far from definitive, the available data are consistent with experiments in mice where bacterial clearance after genital *Ct* or *Cm* infection is known to require T_{H1} cells (31, 37, 38). Mouse experiments have also shown that during *Ct* or *Cm* infection, naive T cells (T_N) differentiate into effector T cells (T_{Eff}) in uterus-draining lymph nodes (LNs), and these T_{Eff} are then recruited to the genital mucosa to mediate bacterial clearance (39-41). T_{H1} cells are also a key component of long-term protective memory post infection, although a role for B cells and antibodies has also been reported (42-47).

Our analysis of UV-*Ct*–cSAP immunized mice revealed a robust *Ct*-specific antibody response that was equivalent to that elicited by *Ct* infection and ~twice as high as in UV-*Ct* exposed mice (**Fig. S3A**). Moreover, i.u. immunization with UV-*Ct*–cSAP increased uterine mucosa-resident CD8 T cells (**Fig. S3B**) as well as CD4 T cells (see below). To ask which component(s) of this multi-facetted response to UV-*Ct*–cSAP was required for mucosal protection we measured bacterial burdens after genital *Ct* infection in vaccinated mutant mice that lacked either B cells (μMt mice, which contain a deletion of the IgM heavy chain) or CD8 T cells ($Cd8^{-/-}$ mice) or CD4 T cells (B6.129S2-$H2^{dlAb1\text{-}Ea}$/J (referred to as MHC-$II^{-/-}$) mice (48)) or both B and T cells ($Rag2^{-/-}$ mice). Neither the absence of B cells nor CD8 T cells had a detectable impact on bacterial levels, whereas $Rag2^{-/-}$ mice (**Fig. S4**) and MHC-$II^{-/-}$ mice were completely unprotected against *Ct* challenge (**Fig. 3A**). Of note, unlike wildtype animals, mice that were devoid of CD4 T cells did not suffer increased bacterial burdens after UV-*Ct* conditioning, indicating that $CD4^+$ T cells are not only needed for pathogen clearance but also for UV-*Ct* induced tolerance.

Since the above experiments demonstrated that CD4 T cells are required for the sequelae of both UV-*Ct* and UV-*Ct*–cSAP exposure, we asked whether CD4 T cells alone were sufficient to confer these effects. Thus, we adoptively transferred purified leukocyte subsets from immunized mice to naïve recipients that were subsequently challenged with *Ct*. Partial protection against genital *Ct* challenge was achieved after transferring 1×10^7 splenic CD4 T cells from mice that had received i.u. injections of either *Ct* or UV-*Ct*–cSAP, whereas transfer of CD8 T cells or T cell depleted splenocytes had no effect (**Fig. 3B**). Transfer of CD4 T cells from UV-*Ct* conditioned donors conferred enhanced susceptibility to infection.

Having determined that CD4 memory T cells are both necessary and sufficient for *Ct*-specific protective memory, as well as tolerance, following immunization with UV-*Ct*-cSAP and UV-*Ct*, respectively, we asked how *Ct*-specific CD4 T_N respond to either stimulus, as compared to *Ct* infection. To this end, T_N from CD90.1$^+$ transgenic NR1 mice (40), in which most CD4 T cells express a *Ct* specific TCR (**Figs. S5**), were adoptively transferred into groups of congenic (CD90.2$^+$) hosts that were subsequently immunized i.u. with *Ct*, UV-*Ct* or UV-*Ct*–cSAP. Four days later, NR1 cells had responded identically to *Ct* infection and UV-*Ct*–cSAP immunization; they had vigorously proliferated and expanded in the draining LN (**Figs. 3C, D**) and they also accumulated in the uterine mucosa (**Fig. 3E**). Moreover, upon *in vitro* rechallenge with UV-*Ct* pulsed autologous DCs, the vast majority of uterine and LN-resident NR1 cells in both groups produced one or more effector cytokines, including IFN-γ, interleukin (IL)-2, and tumor necrosis factor (TNF)-α (**Fig. 3F**). By contrast, in UV-*Ct* exposed animals, NR1 cells showed less proliferation and accumulation in LNs and uterus and they secreted little or no cytokines, similar to T_N.

Mucosal exposure UV-*Ct* generates *Ct* specific regulatory T cells

Although the encounter of UV-*Ct* evoked a blunted T_{Eff} response by *Ct*-specific CD4 T cells, this effect alone cannot explain why UV-*Ct* enhanced host susceptibility to subsequent *Ct* infection. The apparent tolerogenicity of UV-*Ct* clearly depended on CD4 T cells, since UV-*Ct* did not tolerize MHC-II$^{-/-}$ mice (**Fig. 3A**), while adoptive transfer of CD4 T cells from UV-*Ct* conditioned wildtype mice conferred tolerance to naive recipients (**Fig. 3B**). Thus, we hypothesized that mucosal UV-*Ct* exposure may not only compromise T_{Eff} differentiation of *Ct*-specific T_N, but also instigate an alternative "career decision", driving CD4 T_N to differentiate into FoxP3$^+$CD25$^+$ regulatory T cells (Treg). To test this idea, we adoptively transferred to naïve hosts T_N from NR1xFoxP3-eGFP donors after sorting the enhanced green fluorescent protein (eGFP) negative fraction (i.e. non-Treg). Recipients were then immunized with live *Ct*, UV-*Ct* or UV-*Ct*–cSAP. Indeed, there was a massive increase in FoxP3-eGFP$^+$CD25$^+$ NR1 cells in the draining LNs (**Figs. 4A, B**) and uterus (**Figs. 4C, D**) of UV-*Ct* exposed mice, while very few NR1 cells assumed a Treg phenotype in response to *Ct* infection or UV-*Ct*–cSAP vaccination. Since *a priori* eGFP$^+$ Treg had been removed prior to T_N transfer, the appearance of eGFP$^+$ Treg after UV-*Ct* exposure was due to conversion of conventional T_N, rather than expansion of existing Treg. These newly induced Tregs were required for tolerance to *Ct* infection, because anti-CD25 mediated Treg depletion in UV-*Ct* treated mice reduced uterine *Ct* burden upon subsequent infection to levels comparable to naive mice (**Fig. 4E**). Moreover, UV-*Ct* conditioned *Il10*$^{-/-}$ mice did

not suffer enhanced bacterial burdens upon i.u. *Ct* challenge (**Fig. 4F**), suggesting that the *de novo* induced *Ct*-specific Treg exerted their tolerogenic activity through the IL-10 pathway.

Differential mucosal antigen uptake and presentation by uterine dendritic cell subsets

What mechanisms are responsible for the differential T cell response to *Ct* or UV-*Ct*–cSAP *versus* UV-*Ct*? To address this question, we examined the phenotype and function of the three predominant uterus-resident MHC-II$^+$ leukocyte populations (**Fig. S6A**): F4/80$^+$CD11b$^+$ macrophages that were CD11c$^{-/low}$, CD103$^-$ and expressed variable levels of CX3CR1 and two equally sized subsets of CD11c$^+$F4/80$^-$ DCs. One DC subset was CD103$^+$ and expressed neither CD11b nor CX3CR1, while the second DC population was CD103$^-$CD11b$^+$CX3CR1$^+$ (**Fig. S6B**). All three populations were negative for CD207/Langerin and CD301b. Each of these candidate Ag presenting cells (APCs) were sorted from single-cell suspensions of uteri or draining LNs of naive and challenged mice and tested for *Ct* content and ability to stimulate NR1 T_N *in vitro* and *in vivo* (**Fig. 5A**). At 18h after i.u. exposure to *Ct*, UV-*Ct* or UV-*Ct*–cSAP, uterine APCs had not changed significantly in total number or composition (**Figs. S6C, S6D**), and the amount of *Ct*-derived genetic material (determined by qPCR) acquired by both macrophages and CD326$^+$ mucosal epithelial cells was similar in each group (**Fig. 5B**). By contrast, marked differences were apparent among the two DC subsets: live *Ct* and UV-*Ct*–cSAP were primarily acquired by CD103$^-$ DCs, whereas UV-*Ct* accumulated preferentially in CD103$^+$ DCs. Similarly, at 24h after challenge, when sorted APCs were isolated from uterus-draining LNs, bacterial loads were exclusively detected in CD103$^-$ DCs after genital exposure to *Ct* and UV-*Ct*–cSAP, but not UV-*Ct* (**Fig. 5C**).

Consistent with the differential acquisition of *Ct*-derived genetic material, 3-day co-cultures of purified uterine APC subsets with NR1 T_N revealed that CD103$^-$ DCs were singularly efficient at inducing T cell proliferation when they had been isolated from animals exposed to either *Ct* or UV-*Ct*–cSAP. By contrast, among UV-*Ct* exposed APCs only the CD103$^+$ DCs promoted substantial proliferation of NR1 T cells, whereas macrophages failed to induce T cell proliferation regardless of the immunization regimen (**Fig. 5D**). This differential APC activity was recapitulated when APC subsets were isolated from vaccinated animals and injected into footpads of naive mice that had previously received NR1 T_N; CD103$^-$ DCs, but not CD103$^+$ DCs or macrophages, from *Ct* infected and UV-*Ct*cSAP immunized mice stimulated NR1 T_N proliferation in the recipients' draining LNs (**Fig. 5E**). Footpad injection of sorted CD103$^+$ DCs did not promote a significant *in vivo* response by NR1 cells in this experimental setting, however, when CD103$^+$ DCs were isolated from UV-*Ct* conditioned donors and exposed *in vitro* to NR1 T_N, they uniquely promoted the appearance of FoxP3$^+$CD25$^+$ Treg (**Fig. 5F**).

In line with these functional observations, 18h after *Ct* infection or UV-*Ct*-cSAP immunization, uterine CD103$^-$ DCs preferentially upregulated immunostimulatory molecules, including CD80, CD86 and IL-12 (**Figs. 5G, S6E**). In contrast, upon immunization with UV-*Ct*, CD103$^+$ DCs selectively upregulated certain anti-inflammatory pathways, including PD-L2 and IL-10. However, other markers of tolerogenic APCs

remained either unchanged or were undetectable on uterine CD103$^+$ DCs, such as PD-L1 and RALDH, respectively.

We conclude that following mucosal exposure to live *Ct* and UV-*Ct*–cSAP, antigenic material is preferentially acquired and transported to the draining LNs by local immunostimulatory CD103$^-$ DCs, whereas exposure to UV-*Ct* results in Ag acquisition by a tolerogenic DC subset that expresses CD103, leading to the induction of Tregs that then shift the balance from protection to long-lived tolerance in the genital mucosa. Of note, a similar division of labor between CD103$^+$ and CD103$^-$ DCs has been described for the induction of intestinal tolerance and immunity, respectively (49). The differential Ag uptake by intestinal DC subsets is regulated by other mucosa-resident cell types (50-52), however, the mechanism(s) that regulate(s) differential Ag acquisition by uterine DCs remain(s) to be identified.

The route of administration determines UV-*Ct*–cSAP vaccine efficacy

Having established that targeting of uterine CD103$^-$ DCs by transcervical application of UV-*Ct*–cSAP generates long-term protection against genital *Ct* infection, we asked whether other routes of immunization could recapitulate this effect. Thus, mice were immunized with UV-*Ct*–cSAP either s.c. or i.n. and then challenged by i.u. *Ct* infection. Consistent with our experiments using mixtures of UV-*Ct* with conventional adjuvants (**Fig. 1C**), s.c. immunization with live *Ct* or UV-*Ct*–cSAP failed to protect (**Fig. 6A**). By contrast, exposure of nasopharyngeal mucosa to live *Ct* or UV-*Ct*–cSAP rendered mice resistant to genital *Ct* infection akin to i.u. immunization, and this cross-mucosal protective effect persisted unabated for at least 6 months (**Fig. S7**). Interestingly, unlike i.u. conditioning with UV-*Ct*, neither i.n. nor s.c. exposure to UV-*Ct* enhanced the animals' susceptibility to genital *Ct* challenge, suggesting that the rules that govern regional immunity *versus* tolerance in the uterus may be distinct.

Rapid seeding of uterine mucosa with resident memory T cells (T_{RM}) after mucosal but not subcutaneous UV-*Ct*–cSAP vaccination

The fact that percutaneous immunization was ineffective, while vaccination via two distant mucosal routes generated potent protection against genital *Ct* infection, implied that protective CD4 T cells required priming in a MALT environment for efficient mucosal targeting (12). To further investigate this idea, we adoptively transferred 1×10^4 NR1 T_N into mice that were then immunized via different routes with UV-*Ct*–cSAP. Regardless of immunization route, the burst size of NR1 T_{Eff} in peripheral blood was equivalent in magnitude and peaked on day 5 (**Fig. 6B**). Similarly, 7 days and 30 days after i.n., s.c. or i.u. vaccination NR1 cells were equally represented in blood, spleen, LNs and liver, indicating that the route of immunization did not affect the differentiation or trafficking of T_{Eff} and memory cells to these non-mucosal sites (**Fig. 6C**). By contrast, i.u. and i.n. immunization generated Ag-experienced NR1 cells in the lung and uterus, while s.c. vaccination failed to generate mucosa-resident T_{Eff} (**Fig. S8A-C**). A closer examination of the kinetics of uterine T_{Eff} recruitment showed that NR1 T_{Eff} numbers increased gradually after i.n. vaccination, reaching a plateau on day 7. By contrast, i.u. vaccination resulted in a larger peak of uterus-resident NR1 cells on day 7 followed by contraction of the resident T cell pool over the next

several day (**Fig. 6D**). By day 9, both mucosal vaccination strategies had elicited roughly similar uterus-resident T cell numbers, whereas NR1 cells remained essentially undetectable in uteri of s.c. immunized mice.

A critical protective role for uterine T_{RM} upon transcervical *Ct* challenge

The above results suggested that two distinct pools of *Ct*-specific memory T cells were induced: One population was modest in size and consisted of mucosa-resident memory cells (T_{RM}) that arose from T_{Eff} that accessed the uterus early after mucosal (but not s.c.) priming. The pronounced spike in early NR1 T_{Eff} accumulation that was seen after i.u. (but not i.n.) vaccination was presumably a consequence of local tissue irritation that spurred inflammatory recruitment signals in the uterus. It is unlikely that i.n. vaccination altered the steady-state milieu in the uterus, so the fact that uterine T_{Eff} numbers increased steadily during the first seven days post i.n. vaccination suggests the presence of constitutive mucosal recruitment signals for circulating T_{Eff}. While the nature of these steady-state signals remains to be elucidated, our results indicate that T_{Eff} were selectively 'imprinted' by mucosal (i.e. uterine or nasopharyngeal) APCs to engage this uterine recruitment pathway, whereas T_{Eff} generated in skin-draining LNs apparently lacked the prerequisite traffic molecule(s) for uterine homing. Moreover, the longevity of protection after i.n. vaccination (**Fig. S7**) indicates that T_{Eff} that accessed the uterus gave rise to T_{RM} that persisted for at least six months without requiring the presence of local Ag.

The second vaccine-induced memory cell population was much larger than the uterus-resident T_{RM} and resided in blood and lymphoid tissues where these cells are thought to survey the body for recall Ag (53). Although systemic memory cells were elicited by all immunization routes, their protective capacity may vary due to differential imprinting of mucosal homing pathways during the priming phase (2-4, 54, 55). For example, recent work has shown that protective CD4 T cells require the α4β1 integrin to access uterine mucosa (56). We made use of this fact to assess the relative contribution by each memory pool to the clearance of a recurrent *Ct* infection (**Fig. 6E**). To this end, we adoptively transferred NR1 T_N into three groups of mice that then received i.n. UV-*Ct*–cSAP vaccination. Three days later, when activated NR1 T_{Eff} first appeared in the blood, animals in group 1 were given rat IgG every 48h and served as controls in which memory cells had continuous access to the uterus; group 2 received injections of a blocking anti-α4 integrin MAb every 48h, thus preventing uterine T cell homing throughout the experiment; group 3 received control IgG from day 3 to 7, allowing the first wave of *Ct*-specific T_{Eff} to seed the uterine mucosa. On day 9, when i.n. vaccinated control mice had established a stable uterine T_{RM} pool (**Fig. 6D**), all groups were either challenged by i.u. inoculation of *Ct* or left unchallenged, and group 3 was then switched to treatment with anti-α4 integrin MAb to prevent the secondary recruitment of circulating memory cells to the uterus. Animals were sacrificed on day 13 after immunization to assess uterine bacterial burden and/or NR1 cell distribution.

As expected (56), α4 integrin blockade in groups 2 and 3 profoundly affected the accumulation of both NR1 and endogenous CD4 T cells in the infected uterus, but had no significant effect on CD4 T cells in the spleen (**Figs. 6F, S9A-C**). However, while continuous MAb treatment in group 2 essentially abrogated NR1 cell trafficking to both

steady-state and infected uteri, the number of uterine NR1 cells in group 3 was significantly higher than in group 2 and equivalent to that in uninfected uteri of group 1. *Ct* infection in group 1 induced a ~5-fold increase in uterine NR1 cells, whereas late inhibition of α4 integrins in group 3 completely prevented this secondary boost in uterine NR1 cell numbers. There was no difference between groups 1 and 3 in challenge-induced BrdU uptake or Ki-67 expression (a marker of ongoing cell division) by NR1 cells, indicating that mucosa-resident and newly recruited memory cells have a similar proliferative capacity (**Fig. S9D**). Thus, the difference in mucosal T cell numbers between *Ct*-challenged animals in group 1 and group 3 likely reflects the α4 integrin dependent influx of circulating T_{Eff} that occurred in response to infection-induced recruitment signals in the uterus (9). By contrast, the difference between groups 2 and 3 provides a measure for the number of vaccine-induced T_{Eff} that accessed the uterus early after priming and prior to *Ct* infection. Remarkably, although the total number of uterus-resident NR1 cells in group 3 was modest, the bacterial burden was reduced by an order of magnitude as compared to naive mice or animals in group 2, which remained completely unprotected (**Fig. 6G**). However, bacterial burdens in group 1 were even further reduced than in group 3, indicating that both tissue-resident and circulating T cells are needed to achieve optimal clearance of *Ct*. These findings confirm that the migration of both tissue-resident and circulating $CD4^+$ T cells into uterine mucosa depend on α4 integrins, presumably the α4β1 heterodimer (56). It is likely that additional trafficking molecules, such as chemokines are involved in a tissue-specific multi-step adhesion cascade for T cell recruitment to normal uterine mucosa (53), but the molecular identity of these constitutive traffic signals remains to be determined.

Circulating memory T cells induced by mucosal vaccination confer partial protection against *Ct* rechallenge

Having documented the protective capacity of mucosal T_{RM}, we next asked whether circulating memory cells can be protective in the absence of pre-existing T_{RM}. To this end, we performed parabiosis surgery to generate pairs of congenic (CD45.1/CD45.2) mice, which establish a shared circulatory system, allowing genetically traceable hematopoietic cells from each animal to access the blood and tissues of a conjoined partner (57). Control experiments showed that CD4 T cell chimerism (the ratio of partner-derived:endogenous cells) in blood was minimal on day 3 post surgery, but approached ~35:65 and 50:50 on days 4 and 5, respectively (**Fig. S10**). Having thus determined that the earliest timepoint for circulating T cells to gain access to a parabiotic partner's tissues is on day ~4 after surgery, we performed a series of timed parabiosis experiments in congenic pairs of $CD90.2^+$ mice, whereby the $CD45.1^+$ animal in each pair was given genetically tagged ($CD90.1^+$) NR1 T_N, and both mice were immunized with UV-*Ct*–cSAP on the following day (day 0). Congenic pairs were subdivided into six groups: two groups underwent parabiosis surgery on day -14 or -1 before immunization and four groups were parabiosed on day 1, 4, 14 or 21 after immunization (**Fig. 7A**). Six weeks after vaccination, the number of uterine NR1 T_{RM} was similar in all parabionts that had been conjoined on or before day 1 (**Fig. 7B**). In contrast, when parabiosis was initiated on day 4 or thereafter the number of NR1 cells in uteri of non-immunized $CD45.2^+$ partners of immunized $CD45.1^+$ animals was equivalent to that in completely naive parabiotic pairs. These results imply that a transient wave of MALT-derived T_{Eff} gave rise to most if not all uterine T_{RM} within the first 7 days after

immunization. Little or no further T cell recruitment to the uterus occurred after this timepoint. These findings are in perfect agreement with the timecourse of T_{Eff} accumulation in uteri of conventional mice, which increased until day 7 and plateaued thereafter (**Fig. 6D**).

To assess the protective capacity of the circulating memory subset, we devised a modification of the above protocol (**Fig. 7C**), whereby two groups of congenic mice were paired and each CD45.2$^+$ partner received 1×10^5 NR1 T_N followed by i.n. UV-*Ct*–cSAP vaccination. Animals in group A were vaccinated 2 weeks after parabiosis, while in group B vaccination preceded parabiosis by 2 weeks. After another two weeks, both partners were challenged with *Ct*. Four days later, infected uteri in both vaccinated and naive parabiotic animals had recruited substantial numbers of *Ct*-specific NR1 cells (**Figs. 7D, E**) that exceeded those recovered from unifected uteri of vaccinated mice (**Figs. 6D & 7B**). Uterine NR1 cell recruitment was markedly enhanced in all parabionts in group A, where *Ct*-specific memory cells had been generated after a shared circulation was already established so NR1 T_{RM} could seed uteri of both partners (**Fig. 7D**). By contrast, in group B parabiosis was performed after the early wave of mucosa-seeding T_{Eff} had subsided, so uterus-resident NR1 T_{RM} were restricted to the immunized CD45.2$^+$ partner (**Fig. 7E**), whereas circulating memory cells could equilibrate between both partners. Consequently, both parabionts in group A were effectively protected against genital *Ct* challenge (**Fig. 7F**). By contrast, in group B only the immunized partners were fully protected, while the bacterial burden in non-immunized animals, which harbored only circulating NR1 memory cells were indistinguishable from naive NR1 recipients (**Fig. 7G**). Of note, UV-*Ct*–cSAP vaccination induced a robust humoral response against *Ct* (**Fig. S3A**), whereby circulating antibodies are expected to fully equilibrate in parabiotic pairs. The preferential protection of only the vaccinated parabionts in group B suggests that antibodies provided little or no protection in this experimental setting.

While the above experiments permitted simultaneous assessment of the migratory dynamics and protective function of *Ct*-specific T cells, the experimental protocol required that NR1 T_N were transferred at super-physiologic numbers. To control for potential artifacts of elevated frequencies of *Ct*-specific T cells, we performed timed parabiosis experiments without NR1 cell transfer. To this end, either the CD45.1$^+$ or CD45.2$^+$ partner of each congenic pair was immunized before or after parabiosis surgery and both animals were challenged 4 weeks later with *Ct* i.u. (**Fig. 7H**). When uterine bacterial burden was assessed 6 days later, both partners were fully protected when parabiosis had been performed on or before day 1 after vaccination (**Fig. 7I**). Thus, mucosal UV-*Ct*–cSAP vaccination of animals that could generate both T_{RM} and circulating memory cells elicited similar protection against *Ct* challenge with and without prior adoptive transfer of TCR trangenic NR1 cells and regardless of whether we examined individual mice (compare **Fig. 2A** vs. **6G**) or parabiotic pairs (compare **Fig. 7B** vs. **7D**), indicating that NR-1 cell transfers did not artificially skew the overall vaccine response.

Importantly, when parabiosis was delayed until day 4 or later after vaccination, protection of the non-immunized parabionts was noticeably compromised. These findings strongly support the notion that mucosal seeding by vaccine-induced T_{RM} must occur prior to day 8 post vaccination (**Fig. 7B**) and is essential for full-fledged resistance to genital *Ct* challenge.

However, even when parabiosis of animals that did not receive NR1 T_N was delayed after vaccination until day 4 or later, subsequent *Ct* challenge of non-immunized partners resulted in significantly lower bacterial burdens than when naive parabionts were challenged (**Fig. 7I**). Thus, the circulating memory cells that arose from a polyclonal T cell response provided meaningful, if partial, protection in the absence of T_{RM}, while the analogous experiment after adoptive transfer of NR1 T_N failed to reveal protection by circulating memory cells (**Fig. 7G**). This difference was presumably because conventional naive mice contain much fewer *Ct*-specific T_N than NR1 cell recipients, allowing the latter to rapidly generate a large burst of T_{Eff} after *Ct* challenge that may have masked the activity of circulating memory cells. In aggregate, our results suggest that circulating polyclonal memory T cells that arise after mucosal vaccination can accelerate uterine *Ct* clearance, even in the absence of mucosal T_{RM}. However, consistent with the partial protection afforded by adoptive transfer of sensitized splenic CD4 T cells (**Fig. 3B**), this protective activity is suboptimal.

Mucosal UV-*Ct* exposure generates suppressive Treg in parabiotic partners

Finally, we examined parabiotic pairs in which the $CD45.2^+$ partner had received i.u. conditioning with UV-*Ct*. Remarkably, both partners displayed similar hypersusceptibility to *Ct* regardless of whether parabiosis was initiated before or after UV-*Ct* immunization (**Figs. 7J, K**), indicating that uterus-resident Treg may not be needed for the tolerogenic response to *Ct*. This is in line with observations in a murine colitis model, where tissue-homing of Treg was not required to prevent intestinal inflammation (58).

Mucosal UV-*Ct*–cSAP vaccination confers protection against*Ct* challenge in humanized mice

The above findings in conventional mice were fully reproducible in two cohorts of BLT mice (59) that had been reconstituted with a human immune system from two unrelated donors (60). Human CD4 T cells in both cohorts mounted a vigorous mucosal T_{H1} response to clear uterine infection with two different *Ct* serovars, *Ct-L* and *Ct-E* (**Figs. 8A, B**). Moreover, prime-boost vaccination of naive BLT animals with UV-*Ct*–cSAP given i.n. or i.u. (**Fig. 8C**) was highly effective against subsequent i.u. *Ct* challenge, even when BLT mice were challenged with a different serotype than used for immunization (**Fig. 8D, E**).

Conclusion

In summary, using a mucosal immunization strategy, we have dissected the multi-facetted adaptive immune mechanisms that control murine host responses against genital *Ct* infection after mucosal vaccination with a vaccine candidate, UV-*Ct*-cSAP. Our results indicate that optimal protection after *Ct* challenge requires uterine recruitment of two discrete waves of *Ct*-specific CD4 T cells that are inducible in MALT, but not in skin-draining LNs (**Fig. 8F**). Following an immunostimulatory mucosal priming event, the first wave is composed of recently activated T_{Eff} that give rise to long-lived T_{RM} after trafficking to both inflamed and resting mucosal surfaces. This early migratory wave subsides within ~one week after immunization and depends on a constitutive tissue-specific multi-step adhesion cascade (53) involving α4 integrins and presumably other mucosal traffic signals that remain to be

identified. Concomitantly, MALT-derived *Ct*-responsive T_{Eff} also generate a second population of memory cells that preferentially reside in blood and secondary lymphoid organs. This systemic memory population, which is comprised of the two classical central and effector memory subsets (61), does not appear to access the resting urogenital mucosa, but can be recruited to peripheral tissues, including uterine mucosa, upon the onset of inflammation (62). Although this circulating memory subset contributes to the overall recall response against *Ct*, its protective role is suboptimal in the absence of T_{RM}. In an optimally immunized individual, *Ct* infection triggers rapid release of cytokines, particularly IFN-γ, by the mucosal T_{RM} subset, which promotes pathogen clearance (63). This protective effect of uterine T_{RM} may be amplified by their pro-inflammatory activity that may help recruit circulating memory cells, however, our data show that the tissue-resident memory subset confers substantial protection even when the influx of circulating memory cells is blocked.

Of importance to future *Ct* vaccine trials, our experiments potentially shed light on the decades-old conundrum of how exposure to killed *Ct* in trachoma vaccine trials during the 1960s may have enhanced subsequent *Ct*-induced pathology (25-29). We could provoke a similar hypersusceptibility to *Ct* in our mouse model by exposing mucosal surfaces to UV-*Ct*, an effect that was due to *de novo* induction of *Ct*-specific Treg. After conjugating cSAPs to UV-*Ct* for mucosal immunization, we could not only prevent this tolerogenic effect, but also render mice highly resistant to *Ct* infection, a protective response that was identical in magnitude, longevity and immunological mechanism to the endogenous memory response against genuine *Ct* infection. Moreover our findings in BLT mice indicate that human CD4 T cells can also mount a vigorous mucosal T_{H1} response to clear uterine *Ct* infection, suggesting that cSAP-based mucosal vaccination may also elicit protective immune responses in humans. As cSAPs are fully synthetic and biodegradable nanoparticles that are easily manufactured and well tolerated, they may also offer a powerful and versatile approach for mucosal vaccine development against other challenging pathogens.

Materials and Methods

Mice

C57BL/6 and BALB/c mice, 6-8 weeks old, were purchased from Charles River or The Jackson Laboratory. B6.129S2-$H2^{dlAb1\text{-}Ea}$/J (referred to as MHC class $II^{-/-}$) (48), $CD8^{-/-}$, μMt, $Il10^{-/-}$, $Rag2^{-/-}$ and C57BL6 B6.SJL Ptprca Pep3b/BoyJ ($CD45.1^{+}$) mice were were purchased from The Jackson Laboratory and used at 6–12 weeks of age. CD90.1 NR1 mice (TCR tg mice with specificity for the $CD4^{+}$ T cell antigen *Ct*a1 from *Ct*) were bred in-house. For some experiments, we crossed NR1 and Foxp3eGFP mice (64). For characterization of uterine APC subsets $CXCR3^{GFP/+}$ mice (65) were used. BLT mice were generated in the MGH Humanized Mouse Program by transplanting irradiated *NOD/SCID/*$\gamma c^{-/-}$ mice with human fetal liver stem cells and autologous thymic grafts (59). Reconstituted mice developed a fully human lymphoid compartment within ~13-18 weeks post reconstitution at which stage they were used for immunization or vaccination studies. All experiments were performed in accordance with NIH guidelines and approved by the Institutional Animal Committees of Harvard Medical School and MGH.

Chlamydia infection and detection

Ct serovar L2 (434/Bu), referred to as *Ct*, or servar E (*Ct-E*) or *C. muridarum* (*Cm*) were propagated in McCoy cell monolayers grown in Eagle's MEM (Invitrogen, Grand Island, NY) supplemented with 10% FCS, 1.5 g/l sodium bicarbonate, 0.1 M nonessential amino acids, and 1 mM sodium pyruvate, as described previously (41). Aliquots were stored at −80°C in medium containing 250 mM sucrose, 10 mM sodium phosphate, and 5 mM L-glutamic acid and were thawed immediately prior to use. All mice were treated with 2.5 μg medroxyprogesterone s.c. 7 days prior to immunization to normalize the murine estrous cycle. For UV inactivation, *Ct* or *Cm* suspensions were placed under a UV lamp (15 W) at a distance of 30 cm for 30 min. The efficiency of UV inactivation was always tested by infecting McCoy cell monolayers with an aliquot of UV-inactivated Ct and evaluation of inclusion-forming units. Briefly, 30 hours following infection the media was removed, cells were fixed in ice-cold methanol and permeabilized in PBS with .05% tween. Cells were then stained with 10 μl anti-MOMP antibody and Evans blue counterstain (Pathfinder Diagnostic Kit BioRad) for one hour and were then washed 3 times in PBS-tween. Inclusion-forming units were not observed after UV inactivation of *Ct* or *Cm*.

Intrauterine immunization and challenge were conducted transcervically using an NSET device (ParaTechs) as previously described (31). Briefly, 10μ l of sucrose-phosphate-glutamate media containing 10^6 *Ct* or UV-*Ct* +/− cSAP was placed into the uterus using the NSET pipet tip through the NSET speculum. Subcutaneous immunization was done with a U-100 insulin syringe injecting 10μl of sucrose-phosphate-glutamate media containing 10^6 *Ct* or UV-*Ct* +/− cSAP. As 10^6 *Ct* were lethal for mice when deposited intranasally (data not shown), i.n. immunization was performed with 10^5 *Ct* in 10μl of sucrose-phosphate-glutamate media. *Cm* was administered intravaginally as described previously (6).

To quantify the levels of *Ct* in tissues, we usually used qPCR with 16S primers specific for *Ct*, as described previously (66). Briefly, DNA was isolated from uterus homogenates using the QIAamp DNA mini kit (Qiagen). Mouse GAPDH DNA and *Chlamydia* 16S DNA were quantified by qPCR on an ABI Prism 7000 sequence detection system. Using standard curves from known amounts of *Ct* and mouse DNA, the amount of *Chlamydia* DNA (in pg) per unit weight of mouse DNA (in μg) was calculated to assess bacterial burden.

Titers of inclusion-forming units were determined in two experiments. Mouse uteri were disrupted using a tissue homogenizer and frozen at −80C. Aliquots were thawed and tenfold dilutions of each sample were made in a 96 well plate. Each dilution was then used to infect a confluent monolayer of McCoy cells in a 96 well plate by centrifugation for 1 hour at 37C. Two hours following centrifugation media was supplemented with 25ug/ml of gentamicin to prevent contamination. 30 hours following infection the media was removed, cells were fixed in ice cold methanol and permeabilized in PBS with .05% tween. Cells were then stained with 10ul anti-MOMP antibody and evans blue counterstain (Pathfinder Diagnostic Kit BioRad) for one hour then were washed 3 times in PBS-tween. Total inclusions in each sample were then enumerated by fluorescence microscopy with at least 3 fields being counted per sample.

The impact the cSAP constructs on chlamydia-induced pathology of the upper genital tract was measured 4 weeks after Cm challenge of immunized mice and naïve controls. Gross pathology was scored by hydrosalpinx development as follows: 0: normal; 1: low-level fluid in oviduct; 2: moderate amount of fluid present; 3: high level of fluid.

Vaccine formulation

Synthesis of polymers and formulation of synthetic nanoparticles (SPs) was performed as described previously (32) with minor modifications. Briefly, the triblock copolymer poly(d,l-lactic-*co*-glycolic acid)-*b*-poly(l-histidine)-*b*-poly(ethylene glycol) (PLGA-PLH-PEG, referred to as charge-switching synthetic particles, cSPs) was synthesized using a polymer end grafting strategy. Control SPs that lacked the PLH block were formulated in a similar manner using PLGA-PEG copolymers. R848-PLA was synthesized by ring opening polymerization (33). All SPs were formulated using a modified emulsion/solvent evaporation technique. R848-PLA was added in a 0.4:0.4:0.2 (R848-PLA:PLGA-PLH-PEG:PLGA-PEG) ratio. The polymer-containing ethyl acetate solution was sonicated into 2 mL of pure water using a probe tip sonicator (Misonix Sonicator S-4000, Farmingdale, NY) for 30 sec in continuous mode at 40% amplitude then diluted into 8 mL of pure water under magnetic stirring in a fume hood. The solvent was allowed to evaporate for at least 2 hours, at which point SPs were collected and purified by repeated ultrafiltration using Amicon Ultra-4 100,000 NMWL cutoff filters (Millipore, Billerica, MA). The sizes of *Ct*-SP constructs were determined by dynamic light scattering on a Zetasizer Nano (Malvern Instruments).

SAPs, cSAPs and cSPs were prepared, purified, then resuspended in a dilute pH 6.0 solution and 2×10^7 UV-*Ct* were added per mg SPs. This mixture was then incubated at 37°C for at least 30 minutes in the dark under gentle shaking. To determine SP conjugation to the surface of UV-*Ct*, Ct was labeled with BacLight (Life Technologies, (absorption maximum 581, emission maximum 644) and PLGA-AF488, synthesized using ring-opening polymerization, was blended in to the SPs prior to conjugation with bacteria and analyzed with flow cytometry.

Tissue digestion, flow cytometry and cell sorting

Spleens, lungs, lymph nodes, and livers were cut into small pieces with a sterile scalpel and passed through 40μm mesh filters. Uteri were digested with type XI collagenase (Sigma, St Louis, MO) and DNase I (Sigma) for 30 min at 37°C before passing through 40μm filters. Samples were enriched for lymphocytes by density-gradient centrifugation with NycoPrep™ 1.077 according to the manufacturer's protocol (Axis-Shield).

For flow cytometry analysis or cell sorting, T cells were stained with anti-CD3e (145-2C11; BioLegend), anti-CD4 (RM4-5; BioLegend), anti-CD90.1 (OX-7; BioLegend), anti-CD25 (PC61; BioLegend), anti-Va2 (B20.1; BioLegend), anti-Vb8.3 (1B3.3; BD Biosciences), anti-CD45.1 (104; BioLegend), or anti-CD45.2 (A20; BioLegend). T cell proliferation was measured by anti-Ki-67 (16A8; BioLegend) staining and overnight Bromodeoxyuridine (BrdU) labeling according to the manufacturer's protocol (Life Technologies). DCs were characterized and/or sorted with anti-MHC class II (AF6-120.1; BioLegend), anti-F4/80

(BM8; BioLegend), anti-CD103 (2E7; BioLegend), anti-CD11c (N418; BioLegend), anti-CD11b (M1/70; BioLegend), anti-CD207 (eBioL31; eBioscience), anti-CD301b (URA-1; BioLegend), anti-CD80 (16-10A1; BioLegend), anti-CD86 (GL-1; BioLegend), anti-CD274 (PD-L1) (10F.9G2; BioLegend), anti-CD273 (PD-L2) (TY25; BioLegend), anti-IL-10 (JES5-16E3; BioLegend), and anti-IL-12/IL-23 (C15.6; BioLegend). For intracellular T cell cytokine staining, autologous sorted splenic CD11c$^+$ DCs were pulsed with UV-inactivated EBs for 30 min, washed extensively and added to T cells for 5 h in the presence of brefeldin A (GolgiStop; BD Biosciences). T cells were stained for anti–IFN-γ (XMG1.2; BioLegend) anti–IL-2 (JES6-5H4; BioLegend), and anti–TNF-α (MP6-XT22; BioLegend) Abs after permeabilization with the Cytofix/Cytoperm Plus Kit according to the manufacturer's instructions (BD Biosciences). The absolute cell number in each sample was determined using AccuCheck Counting Beads (Invitrogen). Data were collected on a FACSCanto (BD Biosciences) or a LSRII (BD Biosciences) and analyzed using FlowJo 9.3.2. A FACSAria (BD) was used for cell sorting with Diva software and purity was >98% for all experiments.

Adoptive transfer of leukocyte subsets

Lymph nodes and spleens were collected from naive female CD90.1$^+$ NR1 mice and purified by negative immunomagnetic cell sorting using a mouse CD4$^+$ T-cell isolation kit (~98% CD4$^+$, Miltenyi Biotec). Purity was verified with anti-CD4, anti-Va2 and anti-Vb8.3 stainings. For some experiments, FoxP3^{eGFP+} NR1 cells were depleted before adoptive transfer of FoxP3^{eGFP-} NR1 cells by cell sorting. 1×10^5 isolated NR1 cells (unless noted elsewise) were intravenously transferred to naïve recipient mice 1 day prior immunization. In proliferation experiments, NR1 cells were labeled with carboxyfluorescein succinimidyl ester (CFSE) before transfer. For adoptive transfer of polyclonal CD4$^+$ and CD8$^+$ T cells and T cell-depleted leukocytes, cell subsets from immunized mice were harvested from donor spleens by immunomagnetic cell sorting (Miltenyi Biotec) and 10^7 cells were transferred to naïve recipients.

NR1 T cell stimulation by APCs

APCs were isolated from single-cell suspensions of uterus and draining LNs 18 and 24 hours post-immunization, respectively. CD45$^+$MHC class II$^+$ cells were FACS sorted based on their CD103 and F4/80 expression (CD103$^-$F4/80$^+$ macrophages, CD103$^-$F4/80$^-$ DCs and CD103$^+$F4/80$^-$ DCs). Sorted cells were either subjected to qPCR analysis for *Ct* 16S content or co-cultured with CFSE-labeled NR1 cells for 3 days (500 DCs and 5,000 NR-1 cells). For *in vivo* assessment of APC function, naïve mice received 1×10^5 CFSE-labeled NR1 cells i.v. followed one day later by s.c. injection into the right footpad of 5,000 sorted APCs. CFSE-dilution of NR1 cells in the right popliteal LN was analyzed 3 days later.

In vivo MAb treatment

250μg anti-CD25 (PC61) mAb or control IgG were administrated intraperitoneally at days −3 and +3 of uterine *Ct* challenge. Anti-a4 mAb (PS/2) or control IgG was administrated i.v. at day 3 (100μg) and every second day (50μg) until day 11 thereafter. On d9 mice were challenged i.u. with 10^6 IFU of *Ct*.

Parabiosis

Parabiosis surgery was performed as previously described (57). Briefly, sex- and weight-matched congenic partners were anaesthetized with ketamine (100 mg/kg body weight) and xylazine (10 mg/kg body weight) by i.p. injection. The corresponding lateral aspects of mice were shaved and the excess hair was wiped off with alcohol prep pad. Two matching skin incisions were made from the olecranon to the knee joint of each mouse, and the subcutaneous fascia was bluntly dissected to create about 0.5 cm of free skin. The olecranon and knee joints were attached by a double 4-0 braided silk suture and tied, and the dorsal and ventral skins were approximated by staples or continuous 6-0 braided silk suture. The mice were then kept on heating pads and continuously monitored until recovery. 2.5μg g^{-1} flunixin was used for analgesic treatment by subcutaneous injection every 12h for 48h after the operation. After 3 days to 2 weeks, chimerism of leukocytes from the blood was analyzed monitored to ensure equivalent blood exchange between parabiotic partners. Depending on the readout of the experiments, either one of the partners was immunized with UV-*Ct*–cSAP i.n. or UV-*Ct* i.u. and both were challenged with *Ct* i.u., or 10^5 NR1 cells were i.v. injected the day before immunization with UV-*Ct*–cSAP i.n. without further challenge.

Anti-*Ct* Ab ELISA

Antibody levels were determined by enzyme-linked immunosorbent assays (ELISA) using a mouse *Ct* antibody ELISA Kit (MyBioSource). Mice were bled 4 weeks after immunization in order to assess antibody levels.

Confocal and electron microscopy

Uterine tissue was incubated overnight in phosphate-buffered *L*-lysine with 1% paraformaldehyde/periodate and then cryoprotected by subsequent incubations in 10%, 20%, and 30% sucrose in PBS at room temperature, snap-frozen in TBS tissue-freezing liquid (Triangle Biomedical Sciences) and stored at −80°C. Sections of 30μm thickness were mounted on Superfrost Plus slides (Fisherbrand) and stained with anti-CD90.1 PE (OX-7, BD Biosciences), anti-CD326 FITC (G8.8: BioLegend) and anti-CD31 (390, BioLegend) in a humidified chamber after Fc receptor blockade with 1 mg/ml^{-1} antibody 2.4G2 (BD Pharmingen). Samples were mounted in FluorSave reagent solution (EMD-Calbiochem) and stored at 4°C until analysis. Images were acquired with an Olympus Fluoview BX50WI inverted microscope and were analyzed by using Volocity software (Improvision).

Transmission electron microscopy (TEM) samples were prepared using the Gatan Cryo-Plunge3 and imaged using a JEOL 2100 FEG electron microscope.

Statistical analysis

Statistical significance was determined between two groups with two-tailed *t*-test. Statistical differences among three or more groups were assessed using one-way or two-way analysis of variance followed by Bonferroni's post-test to account for multiple comparisons. Significance was set at a *P* value of less than 0.05.

Supplementary Material

Refer to Web version on PubMed Central for supplementary material.

Acknowledgements

We thank E. Nigro for secretarial assistance, L. B. Jones for technical support and the members of the von Andrian laboratory for discussion. The data presented in this manuscript are tabulated in the main paper and in the supplementary materials. This work was supported by National Institutes of Health (NIH) grants AI078897, AI069259, AI095261 and AI111595, a Harvard Innovation Award from Sanofi Pasteur and the Ragon Institute of MGH, MIT and Harvard (to U.H.v.A.), NIH grants U54-CA119349, U54-CA151884, R37-EB000244 and the David Koch-Prostate Cancer Foundation (to R.L. and O.C.F.), NIH grant 1 R01-EB015419-01 (to O.C.F.), NIH grant R00 CA160350 to J. S., NIH grant P30-AI060354 and the MGH Humanized Mouse Program by the Harvard University CFAR (to A.M.Y.). NIH grant R01 AI062827, NIH grant R01 AI39558 and the Epidemiology and Prevention Interdisciplinary Center for Sexually Transmitted Diseases (NIH grant U19 AI113187) (to M.N.S). G. S. is a Max Kade foundation postdoctoral research exchange grant recipient. A.F.R.-M. acknowledges support from the MIT Portugal Program and the National Science Foundation (NSFGRFP). G. S., A. R.-M., P. B., M. S., R. L., O. C. F., U. H. v. A. are inventors on a patent application entitled “Nanoparticle-Based Compositions” (U.S. Application number PCT2014/029000; International Publication No. WO2014/153087) filed by Harvard University together with MIT and Brigham and Women's Hospital (BWH) that relates to the use of cSAP for mucosal vaccination. A. R.-M., R. L., O. C. F. are inventors on a patent application entitled “pH Sensitive Biodegradable Polymeric Particles for Drug Delivery” (U.S. Application number PCT2011/0065807) filed by BWH together with MIT that relates to the engineering of charge-switching particles. O. C. F., R. L. and U. H. v. A. disclose financial interests in BIND Therapeutics, Selecta Biosciences, and Blend Therapeutics, three biotechnology companies developing nanocarrier technologies for medical applications. BIND, Selecta, and Blend did not support the research in this study. Selecta and Blend have obtained licenses to a portion of the intellectual property described in this study. O. C. F., R. L. and U. H. v. A. are scientific founders and members of the Scientific Advisory Board and O. C. F. and R. L. are Directors of Selecta Biosciences. O. C. F., R. L. and U. H. v. A. are members of the Scientific Advisory Board and O. C. F. and R. L. are scientific founders and Directors of Blend Therapeutics. The following reagents used in the paper are subject to MTA: NR-1 transgenic mice, cSAP, cSP and SAP. All reasonable requests for collaboration involving materials used in the research will be fulfilled provided that a written agreement is executed in advance between BWH, MIT, or Harvard Medical School and the requester (and his or her affiliated institution). Such inquiries or requests for additional data should be directed to the corresponding author.

Bibliography

1. Holmgren J, Svennerholm AM. Vaccines against mucosal infections. Curr Opin Immunol. 2012; 24:343–353. [PubMed: 22580196]
2. Mora JR, et al. Selective imprinting of gut-homing T cells by Peyer's patch dendritic cells. Nature. 2003; 424:88–93. [PubMed: 12840763]
3. Mora JR, et al. Generation of gut-homing IgA-secreting B cells by intestinal dendritic cells. Science. 2006; 314:1157–1160. [PubMed: 17110582]
4. Sigmundsdottir H, et al. DCs metabolize sunlight-induced vitamin D3 to ‘program’ T cell attraction to the epidermal chemokine CCL27. Nat Immunol. 2007; 8:285–293. [PubMed: 17259988]
5. Guy-Grand D, Griscelli C, Vassalli P. The mouse gut T lymphocyte, a novel type of T cell. Nature, origin, and traffic in mice in normal and graft-versus-host conditions. J. Exp. Med. 1978; 148:1661–1677. [PubMed: 31410]
6. Kantele A, Zivny J, Hakkinen M, Elson CO, Mestecky J. Differential homing commitments of antigen-specific T cells after oral or parenteral immunization in humans. J Immunol. 1999; 162:5173–5177. [PubMed: 10227989]
7. Campbell DJ, Butcher EC. Rapid acquisition of tissue-specific homing phenotypes by CD4(+) T cells activated in cutaneous or mucosal lymphoid tissues. J. Exp. Med. 2002; 195:135–141. [PubMed: 11781372]
8. Schenkel JM, Fraser KA, Vezys V, Masopust D. Sensing and alarm function of resident memory CD8(+) T cells. Nat Immunol. 2013; 14:509–513. [PubMed: 23542740]
9. Schenkel JM, et al. T cell memory. Resident memory CD8 T cells trigger protective innate and adaptive immune responses. Science. 2014; 346:98–101. [PubMed: 25170049]

10. Gebhardt T, et al. Memory T cells in nonlymphoid tissue that provide enhanced local immunity during infection with herpes simplex virus. Nat Immunol. 2009; 10:524–530. [PubMed: 19305395]
11. Bergsbaken T, Bevan MJ. Proinflammatory microenvironments within the intestine regulate the differentiation of tissue-resident CD8(+) T cells responding to infection. Nat Immunol. 2015; 16:406–414. [PubMed: 25706747]
12. Bienenstock J. The mucosal immunologic network. Annals of allergy. 1984; 53:535–540. [PubMed: 6391284]
13. Gallichan WS, Rosenthal KL. Long-lived cytotoxic T lymphocyte memory in mucosal tissues after mucosal but not systemic immunization. J Exp Med. 1996; 184:1879–1890. [PubMed: 8920875]
14. Santosuosso M, et al. Mechanisms of mucosal and parenteral tuberculosis vaccinations: adenoviral-based mucosal immunization preferentially elicits sustained accumulation of immune protective CD4 and CD8 T cells within the airway lumen. J Immunol. 2005; 174:7986–7994. [PubMed: 15944305]
15. Lee HK, et al. Differential roles of migratory and resident DCs in T cell priming after mucosal or skin HSV-1 infection. J Exp Med. 2009; 206:359–370. [PubMed: 19153243]
16. Shin H, Iwasaki A. A vaccine strategy that protects against genital herpes by establishing local memory T cells. Nature. 2012; 491:463–467. [PubMed: 23075848]
17. Lycke N. Recent progress in mucosal vaccine development: potential and limitations. Nat Rev Immunol. 2012; 12:592–605. [PubMed: 22828912]
18. van Ginkel FW, et al. Enterotoxin-based mucosal adjuvants alter antigen trafficking and induce inflammatory responses in the nasal tract. Infect Immun. 2005; 73:6892–6902. [PubMed: 16177369]
19. Lawson LB, Norton EB, Clements JD. Defending the mucosa: adjuvant and carrier formulations for mucosal immunity. Curr Opin Immunol. 2011; 23:414–420. [PubMed: 21511452]
20. Belland R, Ojcius DM, Byrne GI. Chlamydia. Nat Rev Microbiol. 2004; 2:530–531. [PubMed: 15248311]
21. Satterwhite CL, et al. Sexually transmitted infections among US women and men: prevalence and incidence estimates, 2008. Sex Transm Dis. 2013; 40:187–193. [PubMed: 23403598]
22. Bakken IJ. Chlamydia trachomatis and ectopic pregnancy: recent epidemiological findings. Curr Opin Infect Dis. 2008; 21:77–82. [PubMed: 18192790]
23. Hu VH, Holland MJ, Burton MJ. Trachoma: protective and pathogenic ocular immune responses to Chlamydia trachomatis. PLoS Negl Trop Dis. 2013; 7:e2020. [PubMed: 23457650]
24. Mabey DC, Hu V, Bailey RL, Burton MJ, Holland MJ. Towards a safe and effective chlamydial vaccine: lessons from the eye. Vaccine. 2014; 32:1572–1578. [PubMed: 24606636]
25. Grayston JT, Woolridge RL, Wang S. Trachoma vaccine studies on Taiwan. Ann N Y Acad Sci. 1962; 98:352–367. [PubMed: 13901337]
26. Woolridge RL, et al. Field trial of a monovalent and of a bivalent mineral oil adjuvant trachoma vaccine in Taiwan school children. Am J Ophthalmol. 1967; 63(Suppl):1645–1650. [PubMed: 6067317]
27. Nichols RL, Bell SD Jr. Haddad NA, Bobb AA. Studies on trachoma. VI. Microbiological observations in a field trial in Saudi Arabia of bivalent rachoma vaccine at three dosage levels. Am J Trop Med Hyg. 1969; 18:723–730. [PubMed: 4897605]
28. Nichols RL, Bell SD Jr. Murray ES, Haddad NA, Bobb AA. Studies on trachoma. V. Clinical observations in a field trial of bivalent trachoma vaccine at three dosage levels in Saudi Arabia. Am J Trop Med Hyg. 1966; 15:639–647. [PubMed: 5941182]
29. Sowa S, Sowa J, Collier LH, Blyth WA. Trachoma vaccine field trials in The Gambia. J Hyg (Lond). 1969; 67:699–717. [PubMed: 5261212]
30. Schachter J. Overview of Chlamydia trachomatis infection and the requirements for a vaccine. Rev Infect Dis. 1985; 7:713–716. [PubMed: 3840910]
31. Gondek DC, Olive AJ, Stary G, Starnbach MN. CD4+ T cells are necessary and sufficient to confer protection against Chlamydia trachomatis infection in the murine upper genital tract. J Immunol. 2012; 189:2441–2449. [PubMed: 22855710]

32. Radovic-Moreno AF, et al. Surface charge-switching polymeric nanoparticles for bacterial cell wall-targeted delivery of antibiotics. ACS Nano. 2012; 6:4279–4287. [PubMed: 22471841]
33. Ilyinskii PO, et al. Adjuvant-carrying synthetic vaccine particles augment the immune response to encapsulated antigen and exhibit strong local immune activation without inducing systemic cytokine release. Vaccine. 2014
34. Batteiger BE, Xu F, Johnson RE, Rekart ML. Protective immunity to Chlamydia trachomatis genital infection: evidence from human studies. J Infect Dis. 2010; 201(Suppl 2):S178–189. [PubMed: 20524235]
35. Geisler WM, Lensing SY, Press CG, Hook EW 3rd. Spontaneous resolution of genital Chlamydia trachomatis infection in women and protection from reinfection. J Infect Dis. 2013; 207:1850–1856. [PubMed: 23470847]
36. Brunham RC. Immunity to Chlamydia trachomatis. J Infect Dis. 2013; 207:1796–1797. [PubMed: 23470849]
37. Brunham RC, Rey-Ladino J. Immunology of Chlamydia infection: implications for a Chlamydia trachomatis vaccine. Nat Rev Immunol. 2005; 5:149–161. [PubMed: 15688042]
38. Farris CM, Morrison RP. Vaccination against Chlamydia genital infection utilizing the murine C. muridarum model. Infect Immun. 2011; 79:986–996. [PubMed: 21078844]
39. Hawkins RA, Rank RG, Kelly KA. Expression of mucosal homing receptor alpha4beta7 is associated with enhanced migration to the Chlamydia-infected murine genital mucosa in vivo. Infect Immun. 2000; 68:5587–5594. [PubMed: 10992458]
40. Roan NR, Gierahn TM, Higgins DE, Starnbach MN. Monitoring the T cell response to genital tract infection. Proc Natl Acad Sci U S A. 2006; 103:12069–12074. [PubMed: 16880389]
41. Olive AJ, Gondek DC, Starnbach MN. CXCR3 and CCR5 are both required for T cell-mediated protection against C. trachomatis infection in the murine genital mucosa. Mucosal Immunol. 2011; 4:208–216. [PubMed: 20844481]
42. Morrison SG, Morrison RP. A predominant role for antibody in acquired immunity to chlamydial genital tract reinfection. J Immunol. 2005; 175:7536–7542. [PubMed: 16301662]
43. Li LX, McSorley SJ. B cells enhance antigen-specific CD4 T cell priming and prevent bacteria dissemination following Chlamydia muridarum genital tract infection. PLoS Pathog. 2013; 9:e1003707. [PubMed: 24204262]
44. Brunham RC, Kuo CC, Cles L, Holmes KK. Correlation of host immune response with quantitative recovery of Chlamydia trachomatis from the human endocervix. Infect Immun. 1983; 39:1491–1494. [PubMed: 6840846]
45. Moore T, et al. Fc receptor-mediated antibody regulation of T cell immunity against intracellular pathogens. J Infect Dis. 2003; 188:617–624. [PubMed: 12898452]
46. Farris CM, Morrison SG, Morrison RP. CD4+ T cells and antibody are required for optimal major outer membrane protein vaccine-induced immunity to Chlamydia muridarum genital infection. Infect Immun. 2010; 78:4374–4383. [PubMed: 20660610]
47. Tifrea DF, Ralli-Jain P, Pal S, de la Maza LM. Vaccination with the recombinant major outer membrane protein elicits antibodies to the constant domains and induces cross-serovar protection against intranasal challenge with Chlamydia trachomatis. Infect Immun. 2013; 81:1741–1750. [PubMed: 23478318]
48. Madsen L, et al. Mice lacking all conventional MHC class II genes. Proc Natl Acad Sci U S A. 1999; 96:10338–10343. [PubMed: 10468609]
49. Scott CL, Aumeunier AM, Mowat AM. Intestinal CD103+ dendritic cells: master regulators of tolerance? Trends Immunol. 2011; 32:412–419. [PubMed: 21816673]
50. Mazzini E, Massimiliano L, Penna G, Rescigno M. Oral tolerance can be established via gap junction transfer of fed antigens from CX3CR1(+) macrophages to CD103(+) dendritic cells. Immunity. 2014; 40:248–261. [PubMed: 24462723]
51. McDole JR, et al. Goblet cells deliver luminal antigen to CD103+ dendritic cells in the small intestine. Nature. 2012; 483:345–349. [PubMed: 22422267]
52. Matteoli G, et al. Gut CD103+ dendritic cells express indoleamine 2,3-dioxygenase which influences T regulatory/T effector cell balance and oral tolerance induction. Gut. 2010; 59:595–604. [PubMed: 20427394]

53. von Andrian UH, Mackay CR. T-cell function and migration. Two sides of the same coin. N. Engl. J. Med. 2000; 343:1020–1034. [PubMed: 11018170]
54. Evans DC, et al. Pre-injury polypharmacy as a predictor of outcomes in trauma patients. Int J Crit Illn Inj Sci. 2011; 1:104–109. [PubMed: 22229132]
55. Pipkin ME, et al. Interleukin-2 and inflammation induce distinct transcriptional programs that promote the differentiation of effector cytolytic T cells. Immunity. 2010; 32:79–90. [PubMed: 20096607]
56. Davila SJ, Olive AJ, Starnbach MN. Integrin alpha4beta1 is necessary for CD4+ T cell-mediated protection against genital Chlamydia trachomatis infection. J Immunol. 2014; 192:4284–4293. [PubMed: 24659687]
57. Wright DE, Wagers AJ, Gulati AP, Johnson FL, Weissman IL. Physiological migration of hematopoietic stem and progenitor cells. Science. 2001; 294:1933–1936. [PubMed: 11729320]
58. Denning TL, Kim G, Kronenberg M. Cutting Edge: CD4+CD25+ Regulatory T Cells Impaired for Intestinal Homing Can Prevent Colitis. J Immunol. 2005; 174:7487–7491. [PubMed: 15944246]
59. Brainard DM, et al. Induction of robust cellular and humoral virus-specific adaptive immune responses in human immunodeficiency virus-infected humanized BLT mice. J Virol. 2009; 83:7305–7321. [PubMed: 19420076]
60. Wege AK, Melkus MW, Denton PW, Estes JD, Garcia JV. Functional and phenotypic characterization of the humanized BLT mouse model. Curr Top Microbiol Immunol. 2008; 324:149–165. [PubMed: 18481459]
61. Sallusto F, Lenig D, Forster R, Lipp M, Lanzavecchia A. Two subsets of memory T lymphocytes with distinct homing potentials and effector functions. Nature. 1999; 401:708–712. [PubMed: 10537110]
62. Weninger W, Crowley MA, Manjunath N, von Andrian UH. Migratory properties of naive, effector, and memory CD8(+) T cells. J. Exp. Med. 2001; 194:953–966. [PubMed: 11581317]
63. Masopust D, et al. Dynamic T cell migration program provides resident memory within intestinal epithelium. J Exp Med. 2010; 207:553–564. [PubMed: 20156972]
64. Bettelli E, et al. Reciprocal developmental pathways for the generation of pathogenic effector TH17 and regulatory T cells. Nature. 2006; 441:235–238. [PubMed: 16648838]
65. Jung S, et al. Analysis of fractalkine receptor CX(3)CR1 function by targeted deletion and green fluorescent protein reporter gene insertion. Mol. Cell. Biol. 2000; 20:4106–4114. [PubMed: 10805752]
66. Bernstein-Hanley I, et al. Genetic analysis of susceptibility to Chlamydia trachomatis in mouse. Genes Immun. 2006; 7:122–129. [PubMed: 16395389]

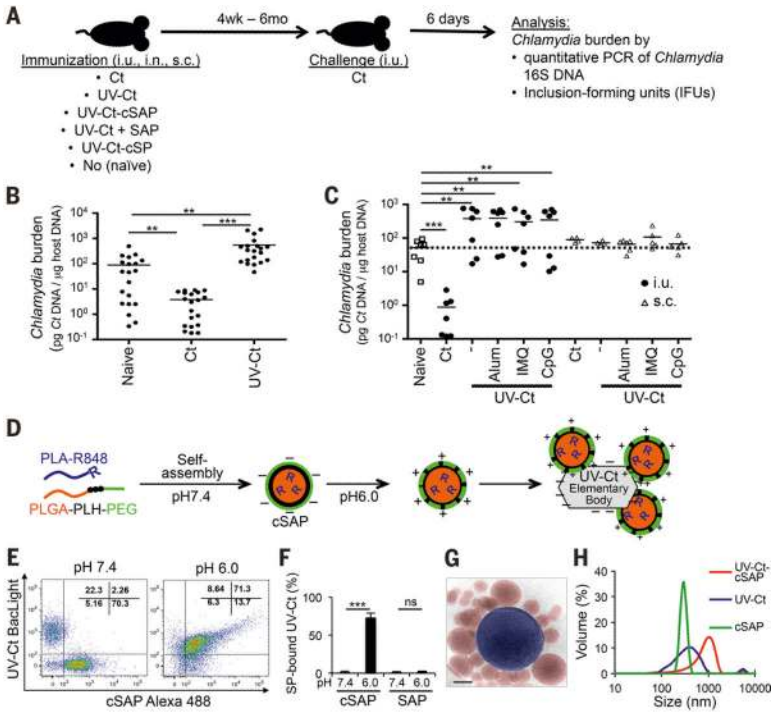

Figure 1. Differential effects of immunization with *Ct* / UV-*Ct* and conjugation of UV-*Ct* with synthetic nanoparticles

(**A**) Schematic diagram of the immunization and challenge protocol for Figs. 1B-C, 2A-C, 2F, 3A-B, 4E-F, 6A, S4 and S7. Mice were immunized with *Ct*, UV-*Ct*, UV-*Ct*-cSAP or UV-*Ct* mixed with control nanoparticles (*Ct*, live *Chlamydia trachomatis*; UV-*Ct*, inactivated *Chlamydia trachomatis*; UV-*Ct*-cSAP, inactivated *Chlamydia trachomatis* complexed with charge-switching synthetic adjuvant particles; UV-*Ct* + SAP, inactivated *Chlamydia trachomatis* mixed with synthetic adjuvant particles (not attached to UV-Ct); UV-*Ct*-cSP inactivated *Chlamydia trachomatis* complexed with charge-switching synthetic particles (without adjuvant)) via intrauterine (i.u.), intranasal (i.n.) or subcutaneous (s.c.) routes. Challenge with live *Ct* was always i.u. (**B**) Uterine *Ct* burden was measured by qPCR 6 days post i.u. challenge with live *Ct* in naïve mice and in animals that had been immunized 4 weeks earlier by i.u. injection of infectious *Ct* or UV-*Ct*. Data are pooled from 4 independent experiments (n= 20 mice per group; ***P*<0.01; ****P*<0.001; one-way ANOVA followed by Bonferroni's post-test). (**C**) *Ct* burden following i.u. or s.c. immunization with UV-*Ct* mixed with adjuvants: alum, aluminum hydroxide; IMQ, imiquimod; CpG, CpG oligodeoxynucleotide type C (n= 5-7 mice per group; ***P*<0.002; ****P*<0.001; one-way ANOVA followed by Bonferroni's post-test). (**D**) Schematic representation of surface charge-switching synthetic adjuvant particle (cSAP) production and conjugation to UV-*Ct*. (**E-F**) UV-*Ct* stained with BacLight was incubated with Alexa Fluor488 labeled cSAP or SAP at pH 7.4 or 6.0. (**E**) Representative FACS plots and (**F**) quantification of nanoparticle conjugates with UV-*Ct* from 2 independent experiments. ****P*<0.001; ns, not significant; two-tailed t-tests. (**G**) A representative cryo-transmission electron micrograph of a UV-*Ct*–cSAP cluster showing cSAP in red and UV-Ct in blue. Scale bar: 100 nm. (**H**) Dynamic light scattering profiles of UV-*Ct*–cSAP, cSAP and UV-*Ct* alone. The population

distribution is representative of the volume scattering intensity. Data are representative of 10 independent experiments. Error bars represent mean ± SEM.

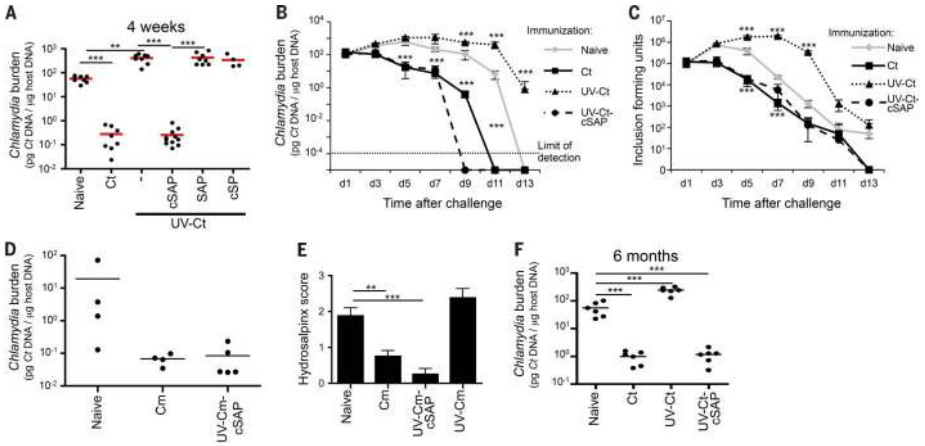

Figure 2. Intrauterine immunization with UV-*Ct*–cSAP protects against challenge with live Ct

(**A**) *Ct* burden following i.u. challenge with live *Ct* 4 weeks after immunization (n=4-10 mice/group; ***P*<0.01; ****P*<0.001). (**B-C**) Timecourse of *Ct* burden following i.u. *Ct* challenge 4 weeks after immunization (n=4 mice/group/timepoint, ****P*<0.001) measured by (**B**) qPCR or (**C**) *in vitro* assessment of inclusion-forming units (IFUs). **(D)** *Ct* burden following intravaginal challenge with *Cm* 4 weeks after immunization with *Cm* and UV-*Cm*-cSAP. n = 3-4 mice/group; *** *P*<0.001. (**E**) Gross uterine pathology determined as hydrosalpinx score 4 weeks after intravaginal challenge of immunized and naïve mice with *Cm* (n=8 mice/group; ***P*<0.01, ****P*<0.001. (**F**) *Ct* burden following i.u. *Ct* challenge 6 months after i.u. im munization (n=4-10 mice/group; ****P*<0.001). Statistical differences were assessed using one-way ANOVA followed by Bonferroni's post-test.

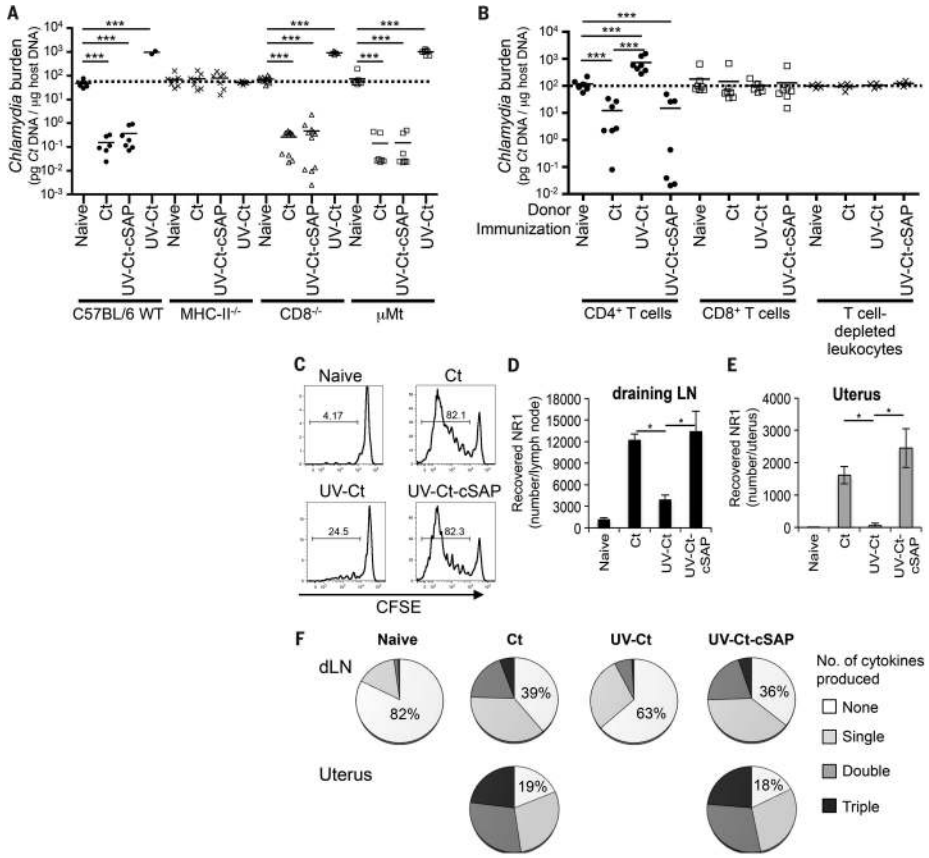

Figure 3. Intrauterine immunization with UV-*Ct* or UV-*Ct*–cSAP leads to differential activation of *Ct*-specific CD4$^+$ T cells

(**A**) *Ct* burden following i.u. *Ct* challenge of MHC-II$^{-/-}$, CD8$^{-/-}$ or µMt mice 4 weeks after immunization (n=2-11 mice/group; ***P<0.001). (**B**) *Ct* burden in i.u. infected mice that received adoptive transfers of leukocyte subsets from naive or immunized donors. Pooled data from 2 independent experiments (n=4-7 mice/group; ***P<0.001). (**C-F**) Flow cytometric analysis of *Ct*-specific NR1 cells in uterus and draining iliac LNs 4 days after i.u. immunization. (**C**) NR1 cell proliferation in uterus draining LNs. Representative histograms show CFSE dilution, a measure of T cell proliferation, in one of three independent experiments. (**D-E**) Absolute number of NR1 cells recovered from (**D**) iliac LNs and (**E**) the uterus. (**F**) Intracellular cytokine staining for TNF-α, IFN-γ, and IL-2 in iliac LN-derived NR1 cells after *ex vivo* restimulation with Ag-pulsed DCs. Data are shown as percentage of total NR1 cells expressing each combination of cytokines (n=5 mice/group; *P<0.05). Statistical differences were assessed using one-way ANOVA followed by Bonferroni's post-test.

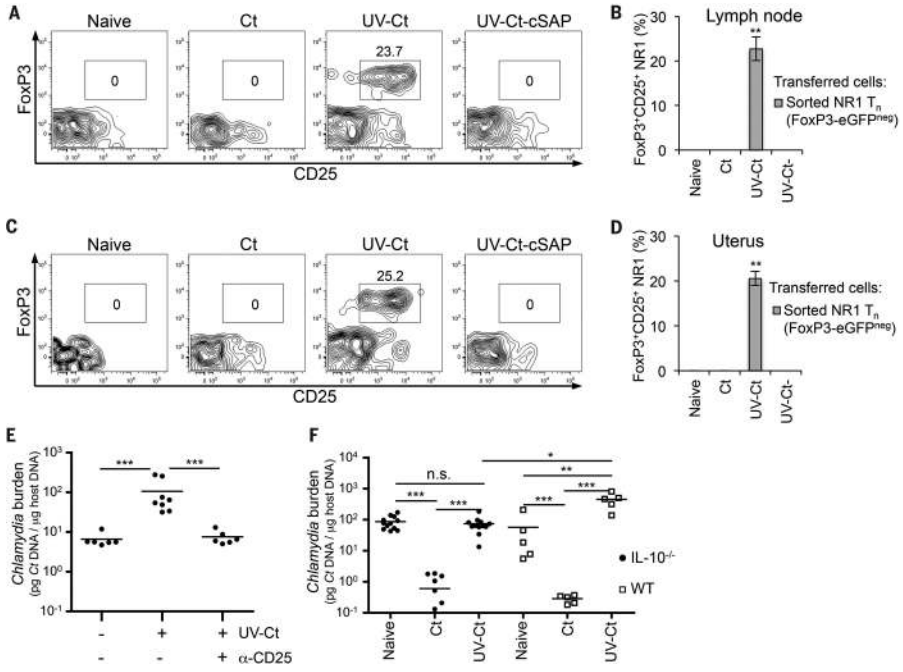

Figure 4. UV-Ct-induced tolerance is mediated by FoxP3$^+$ NR-1 cells

(**A-D**) Sorted GFP$^-$ NR1xFoxP3-eGFP T_N were adoptively transferred to naïve mice prior to immunization. Total GFP$^+$CD25$^+$ NR1 cells (CD4$^+$Vβ8.3$^+$Vα2$^+$) were enumerated by FACS in single-cell suspensions of **(A, B)** iliac LNs and (**C, D**) uterus 4 days after immunization and are shown as (**A, C**) representative contour plots of NR1 cells and (**B, D**) percent of total NR1 cells (n=5 mice/group; ***P*<0.01). **(E)** *Ct* burden following i.u. *Ct* challenge 4 weeks after immunization with *Ct*, UV-*Ct* or UV-*Ct*–cSAP. In some animals Treg were depleted with anti-CD25 mAb (clone PC61), while the other groups received isotype-matched IgG three days before and after challenge (n=6 mice/group; ****P*<0.001). (**F**) *Ct* burden following i.u. challenge with live *Ct* 4 weeks after immunization of *Il10*$^{-/-}$ mice. (n=5-11 mice/group; **P*<0.05; ***P*<0.01; ****P*<0.001). Error bars depict mean ± SEM. Statistical differences were assessed using one-way ANOVA followed by Bonferroni's post-test.

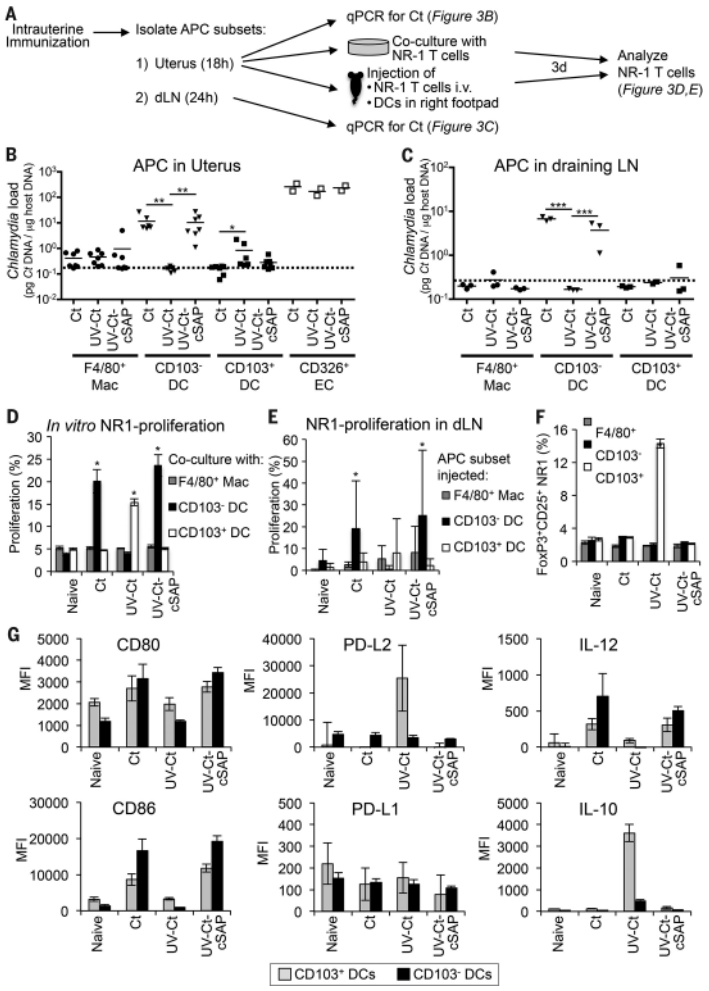

Figure 5. Distinct uterine DC subsets acquire Ags after i.u. *Ct* and UV-*Ct*-cSAP *versus* UV-*Ct* immunization and induce differential responses by *Ct*-specific T cells *in vitro* and *in vivo*

(**A**) Schematic diagram of the experimental protocol for panels **B-F**. Mice were immunized i.u. with *Ct*, UV-*Ct*, or UV-*Ct*–cSAP. At indicated timepoints thereafter, CD45$^+$MHC-II$^+$ APC subsets were isolated from uteri and LNs and FACS sorted based on CD103 and F4/80 expression. Uptake of *Ct* per 1,000 sorted APCs in the uterus (**B**) and draining LN (**C**) was measured by qPCR. Isolated uterine CD326$^+$ epithelial cells (EC) served as positive control for uterine samples. Data are pooled from two independent experiments. Mac, macrophages; DC, dendritic cells. n=2-7; broken line, limit of detection; **P*<0.05; ***P*<0.01; ****P*<0.001. (**D**) *In vitro* proliferation of NR1 T_N was determined by CFSE dilution after incubation with sorted APC subsets for 3 days (n=4 mice/group; **P*<0.05). (**E**) *In vivo* proliferation of CFSE-labeled CD90.1$^+$ NR1 cells in a draining popliteal LN 3 days after footpad injection of APC subsets (n=4 mice/group; **P*<0.05). (**F**) FoxP3-eGFP-depleted NR1 cells were incubated *in vitro* with sorted APC subsets. Frequencies of FoxP3-eGFP$^+$ Treg were determined by flow cytometry after 3 days (n=4 mice/group; **P*<0.05). (**G**) 18 hours after immunization uterine DC subsets were analyzed by FACS for indicated markers (n=4). Error bars represent mean ± SEM. Statistical differences were assessed using one-way ANOVA followed by Bonferroni's post-test.

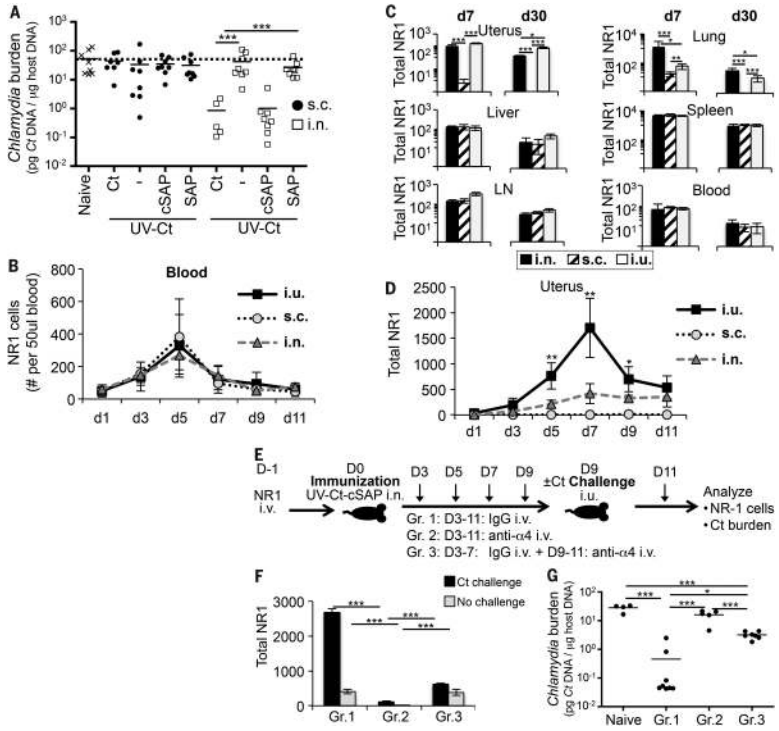

Figure 6. Generation and protective function of uterus-resident and systemic memory T cell subsets induced by intranasal UV-*Ct*–cSAP vaccination

(**A**) *Ct* burden was determined by qPCR following i.u. *Ct* challenge 4 weeks after s.c. or i.n. immunization (n=5-8 mice/group). (**B**) Timecourse of circulating NR1 T_{Eff} during days 1-11 post immunization (n=4 mice/group). (**C**) Total number of NR1 cells recovered from indicated tissues on days 7 and 30 following i.n., s.c. or i.u. immunization. LN, mesenteric lymph node. (**D**) Timecourse of uterine NR1 cell accumulation during days 1-11 post immunization (n=4 mice/group). (**E**) Schematic protocol for timed neutralization of α4 integrins in the 3 groups of *UV-Ct*-cSAP vaccinated mice shown in panels **F-G**. (**F**) Total number of uterus-resident NR1 cells determined by flow cytometry (n=4 mice/group). (**G**) Uterine *Ct* burden 3 days after i.u. *Ct* challenge. Data are from 2 independent experiments; n=4-8 mice/group. Statistical differences were assessed using one-way ANOVA followed by Bonferroni's post-test.

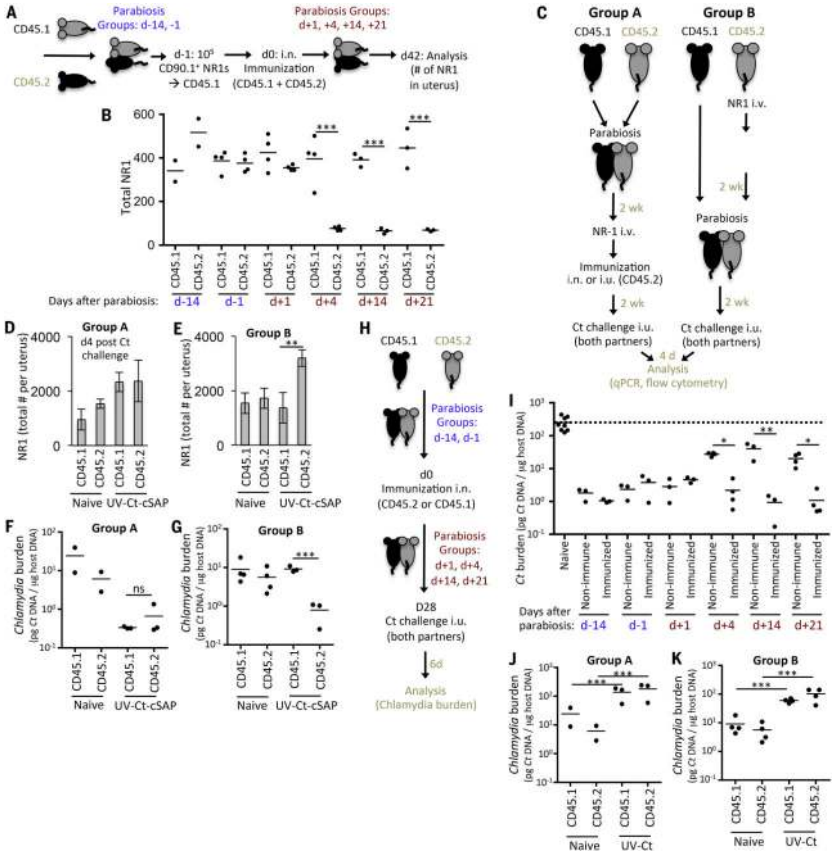

Figure 7. Mucosal UV-*Ct*–cSAP vaccination rapidly induces a transient wave of T_{Eff} that generate protective T_{RM} in uterine mucosa

(**A**) Schematic protocol for timed parabiosis experiments in panel **B**. Parabiosis of CD90.2$^+$CD45.2$^+$ mice with CD90.2$^+$CD45.1 partners was performed on indicated days before or after i.n. immunization of both partners with UV-*Ct*–cSAP. (**B**) On day −1, the CD45.1 animal received 1×10^5 CD90.1$^+$ NR1 T_N and uterine NR1 T_{RM} were counted 6 weeks later (n=2-4 UV-*Ct*-cSAP immunized pairs and 2 naïve parabiotic pairs). (**C**) Schematic protocol for parabiosis experiments in panels **D-G** and **J-K**. CD90.2$^+$CD45.2$^+$ mice were immunized with UV-*Ct*–cSAP i.n. or UV-*Ct* i.u. 2 weeks before or after parabiosis with a CD90.2$^+$CD45.1 partner. 1×10^5 CD90.1$^+$ NR-1 T_N were adoptively transferred to the CD45.2$^+$ animal one day prior to immunization. Animals were either immunized 2 weeks after (group A; panels **D, F, J**) or two weeks before parabiosis surgery (group B; panels **E, G, K**). n = 3 parabiotic pairs immunized with UV-*Ct*-cSAP or UV-*Ct* and 2 naive parabiotic pairs. (**D, E**) Total number of NR1 cells in the uterus 4 days after *Ct* challenge (n = 3 parabiotic pairs immunized with UV-*Ct*-cSAP and 2 naïve parabiotic pairs. **P<0.01). (**F-G**) *Ct* burden 4 days after i.u. *Ct* challenge of both partners in animals that had been conditioned with i.n. UV-*Ct*-cSAP. (**H**) Schematic protocol for timed parabiosis experiments in panel **I**. One partner of each CD45.1/CD45.2 congenic pair was randomly chosen to be immunized on day 0 and underwent parabiosis surgery at indicated timepoints. (**I**) Both parabionts in each pair (n=3-4/group) were challenged i.u. with *Ct* on day 28. Non-immunized parabiotic pairs served as naive controls (n=4). *Ct* burden was assessed 6 days after challenge. All groups were significantly different from naïve parabionts (P<0.05; one-

way ANOVA followed by Bonferroni's post-test.). (**J, K**) Uterine *Ct* burden 4 days after both i.u. *Ct* challenge of parabiotic partners after conditioning with i.n. UV-*Ct*. ***P<0.001; ns, non significant. Error bars show mean ± s.e.m. Unless stated otherwise, statistical differences were assessed using two-tailed *t*-test.

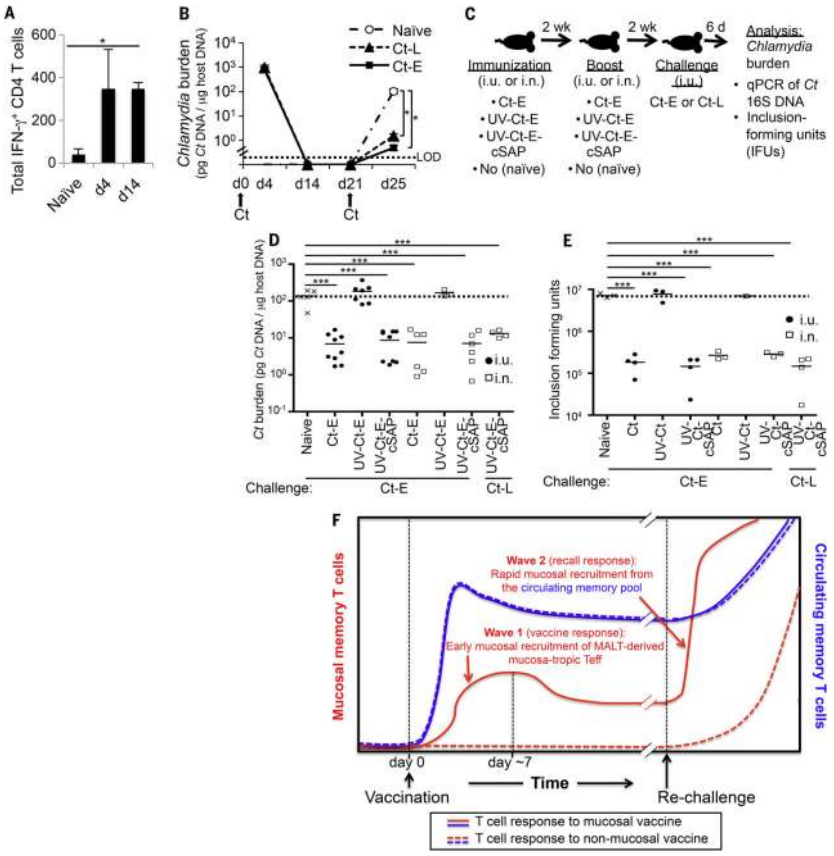

Figure 8. Humanized BLT mice are protected from *Ct* challenge after UV-*Ct*-cSAP immunization

(**A, B**) Immune response of a cohort of humanized BLT mice to uterine infection with *Ct-E* or *Ct-L*. All animals had been reconstituted with human fetal thymus, liver and hematopoietic stem cells from the same donor. (**A**) Number of IFN-γ producing human CD4 T cells per uterus (n = 5 mice/timepoint; **P*<0.05). (**B**) Animals were infected on day 0 and rechallenged on day 21 (arrows). Uterine *Ct* burden was measured on days 4, 14, 21 or 25 by qPCR. LOD, limit of detection; *Ct-E*, *C. trachomatis* serotype E; *Ct-L*, *C. trachomatis* serotype L. n = 2 mice/group. **P*<0.05. (**C**) Schematic protocol for experiments in panels **D** and **E**. These experiments were performed using two cohorts of BLT mice that had been reconstituted with material from different human donors. (**D-E**) BLT mice were left naive or immunized (day 0) and boosted (day 14) as indicated using *Ct* serotype E (*Ct*-E) as immunogen. All animals were challenged with live *Ct*-E or *Ct* serotype L (*Ct*-L) on day 28. *Ct* burden was determined **(D)** by qPCR or **(E)** by measurement of IFUs on day 6 after challenge (n=1-9 mice/group pooled from 2 independent experiments with material from genetically different human donors). **P*<0.05; ***P*<0.01; ****P*<0.001; ns, not significant. Error bars reflect mean ± SEM. (**F**) Schematic summary conclusion. Two waves of vaccine-induced *Ct* specific memory T cells must access the uterine mucosa to confer optimal protection against *Ct* challenge. Mucosal vaccination against *Ct* induces an early burst of circulating T_{Eff} (solid lines) that seed the uterine mucosa during the first week after immunization (wave 1) and give rise to long-lived resident memory T cells. By contrast, non-mucosal vaccines do not induce this first wave of mucosa-tropic memory cells (broken

lines). Regardless of vaccination route, immunized hosts generate circulatory memory T cells, which do not traffic to resting uterine mucosa and are slow to access the re-challenged uterus in the absence of pre-existing T_{RM}. However, in mucosal vaccine recipients uterine T_{RM} can respond instantly to rechallenge with *Ct* and instigate the rapid recruitment of additional *Ct*-specific memory cells from the circulating pool (wave 2). Our results indicate that memory cells from both waves are required for optimal clearance of uterine *Ct* infection. Statistical differences were assessed using one-way ANOVA followed by Bonferroni's post-test.